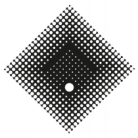
VICTORIA UNIVERSITY
MELBOURNE AUSTRALIA

Single-extracellular vesicle (EV) analyses validate the use of L1 Cell Adhesion Molecule (L1CAM) as a reliable biomarker of neuron-derived EVs

This is the Published version of the following publication

Nogueras-Ortiz, Carlos J, Eren, Erden, Yao, Pamela, Calzada, Elizabeth, Dunn, Christopher, Volpert, Olga, Delgado-Peraza, Francheska, Mustapic, Maja, Lyashkov, Alexey, Rubio, F Javier, Vreones, Michael, Cheng, Lesley, You, Yang, Hill, Andrew F, Ikezu, Tsuneya, Eitan, Erez, Goetzl, Edward J and Kapogiannis, Dimitrios (2024) Single-extracellular vesicle (EV) analyses validate the use of L1 Cell Adhesion Molecule (L1CAM) as a reliable biomarker of neuron-derived EVs. Journal of Extracellular Vesicles, 13 (6). ISSN 2001-3078

The publisher's official version can be found at https://isevjournals.onlinelibrary.wiley.com/doi/10.1002/jev2.12459
Note that access to this version may require subscription.

Downloaded from VU Research Repository https://vuir.vu.edu.au/49379/

Received: 31 October 2023 | Revised: 15 April 2024 | Accepted: 10 May 2024

DOI: 10.1002/jev2.12459

RESEARCH ARTICLE

Single-extracellular vesicle (EV) analyses validate the use of L1 Cell Adhesion Molecule (L1CAM) as a reliable biomarker of neuron-derived EVs

Carlos J Nogueras-Ortiz[1] | **Erden Eren**[1] | **Pamela Yao**[1] | **Elizabeth Calzada**[1] | **Christopher Dunn**[2] | **Olga Volpert**[3] | **Francheska Delgado-Peraza**[1] | **Maja Mustapic**[1] | **Alexey Lyashkov**[1] | **F Javier Rubio**[4] | **Michael Vreones**[1] | **Lesley Cheng**[5] | **Yang You**[6,7] | **Andrew F Hill**[5,8] | **Tsuneya Ikezu**[6,7] | **Erez Eitan**[3] | **Edward J Goetzl**[9,10] | **Dimitrios Kapogiannis**[1,11]

[1]Laboratory of Clinical Investigation, Intramural Research Program, National Institute on Aging, National Institutes of Health (NIA/NIH), Baltimore, Maryland, USA

[2]Flow Cytometry Unit, Intramural Research Program, National Institute on Aging, National Institutes of Health (NIA/NIH), Baltimore, Maryland, USA

[3]NeuroDex Inc., Natick, Maryland, USA

[4]Neuronal Ensembles in Addiction Section, Behavioral Neuroscience Research Branch, Intramural Research Program/National Institute on Drug Abuse/National Institutes of Health, Baltimore, Maryland, USA

[5]La Trobe Institute for Molecular Science, La Trobe University, Bundoora, Victoria, Australia

[6]Department of Neuroscience, Mayo Clinic, Jacksonville, Florida, USA

[7]Department of Pharmacology and Experimental Therapeutics, Boston University School of Medicine, Boston, Massachusetts, USA

[8]Institute for Health and Sport, Victoria University, Melbourne, Victoria, Australia

[9]Department of Medicine, University of California, San Francisco, California, USA

[10]San Francisco Campus for Jewish Living, San Francisco, California, USA

[11]Department of Neurology, Johns Hopkins School of Medicine, Baltimore, Maryland, USA

Correspondence
Dimitrios Kapogiannis, Laboratory of Clinical Investigation, National Institute on Aging (NIA/NIH), 3001 S. Hanover St, 5th floor, Baltimore, MD 21225, USA.
Email: kapogiannisd@mail.nih.gov

Carlos J. Nogueras-Ortiz, Laboratory of Clinical Investigation, National Institute on Aging (NIA/NIH), 251 Bayview Blvd, Baltimore, MD 21224, USA.
Email: carlos.nogueras-ortiz@nih.gov

Abstract

Isolation of neuron-derived extracellular vesicles (NDEVs) with L1 Cell Adhesion Molecule (L1CAM)-specific antibodies has been widely used to identify blood biomarkers of CNS disorders. However, full methodological validation requires demonstration of L1CAM in individual NDEVs and lower levels or absence of L1CAM in individual EVs from other cells. Here, we used multiple single-EV techniques to establish the neuronal origin and determine the abundance of L1CAM-positive EVs in human blood. L1CAM epitopes of the ectodomain are shown to be co-expressed on single-EVs with the neuronal proteins β-III-tubulin, GAP43, and VAMP2, the levels of which increase in parallel with the enrichment of L1CAM-positive EVs. Levels of L1CAM-positive EVs carrying the neuronal proteins VAMP2 and β-III-tubulin range from 30% to 63%, in contrast to 0.8%–3.9% of L1CAM-negative EVs. Plasma fluid-phase L1CAM does not bind to single-EVs. Our findings support the use of L1CAM as

This is an open access article under the terms of the Creative Commons Attribution-NonCommercial License, which permits use, distribution and reproduction in any medium, provided the original work is properly cited and is not used for commercial purposes.
© 2024 Neurodex Inc. and The Author(s). *Journal of Extracellular Vesicles* published by Wiley Periodicals LLC on behalf of International Society for Extracellular Vesicles. This article has been contributed to by U.S. Government employees and their work is in the public domain in the USA.

a target for isolating plasma NDEVs and leveraging their cargo to identify biomarkers reflecting neuronal function.

KEYWORDS
Alzheimer's disease, blood biomarkers, extracellular vesicles, L1CAM, neuron-derived extracellular vesicles

1 | INTRODUCTION

During the last decade, extracellular vesicles (EVs) of presumed neuronal origin have been leveraged as a source of blood biomarkers for neurodegenerative and other brain diseases. The fact that the brain is inaccessible for tissue sampling whilst patients are alive and the invasiveness of even obtaining cerebrospinal fluid for analysis necessitate the development of blood biomarkers reflecting brain pathologies. However, soluble biomarkers for brain diseases typically show low blood concentrations, whereas their concomitant production by peripheral tissues and the brain-blood barrier challenge their attribution to brain cells (Lewczuk et al., 2018). To overcome these conceptual and practical limitations, we and others have developed approaches for the isolation of enriched populations of neuron-derived EVs (NDEVs), the cargo of which would theoretically reflect homeostatic and pathologic processes in their parent cells, akin to a 'liquid biopsy'. We have demonstrated that NDEV-based biomarkers reflect Alzheimer's disease (AD) pathology in mice (Delgado-Peraza et al., 2021) and brain atrophy in humans (Mullins et al., 2017; Walker et al., 2021), and have shown promise as diagnostic biomarkers for clinical and preclinical AD (Fiandaca et al., 2015; Kapogiannis et al., 2019) and as therapeutic response biomarkers for the disease (Delgado-Peraza et al., 2023). Studies from multiple groups have demonstrated the value of this approach for biomarker development for Parkinson's disease (Blommer et al., 2023; Jiang et al., 2020; Shi et al., 2014) and parkinsonian disorders (Dutta et al., 2023), HIV-associated cognitive disorder (Sun et al., 2017), traumatic brain injury (Peltz et al., 2020), multiple sclerosis (Bhargava et al., 2021), depression (Nasca et al., 2021) and schizophrenia (Goetzl et al., 2022; Kapogiannis et al., 2019), among an ever-expanding list of brain disorders.

The conceptual and technical foundation of most of these studies has been the immunoprecipitation (IP) of NDEVs from blood using antibodies targeting the ectodomain of the neuronal membrane protein L1 Cell Adhesion Molecule (L1CAM). The L1CAM IP methodology was first described in two independent reports (Fiandaca et al., 2015; Shi et al., 2014) based on the hypothesis that L1CAM-positive EVs secreted by brain neurons cross the blood-brain barrier (BBB). The rationale was founded upon the following observations: 1) EVs carry molecules expressed by the cell of origin, including membrane proteins that can be targeted via IP for the isolation of cell-specific EVs from complex biofluids (Mitsuhashi et al., 2013; Tauro et al., 2012); 2) L1CAM is readily detectable in EVs secreted by cultured neurons (Faure et al., 2006; Lachenal et al., 2011); 3) genetic signatures of brain tumours are detected in peripheral EVs (Skog et al., 2008), whereas the cargo of EVs injected to the peripheral circulation is detected in the brain (Alvarez-Erviti et al., 2011), suggesting that the BBB is bi-directionally permeable to EVs. These initial studies demonstrated that the L1CAM IP of human serum and plasma recovers nanoparticles containing canonical EV markers, such as Alix and CD81, and proteins highly expressed by neurons, including L1CAM, alpha-synuclein, tau and amyloid beta (Aβ), as illustrated by immunoblots and protein assays (Fiandaca et al., 2015; Shi et al., 2014). Although these neuronal proteins are also expressed by other peripheral organs, the fact that EV levels of Aβ_{42}, Tau phosphorylated at Thr181 and Ser396, and alpha-synuclein recovered via L1CAM IP distinguish patients with AD or PD from controls suggest their derivation from brain areas that show pathology and, indirectly, support the relative (although not absolute) brain specificity of L1CAM+ EVs in blood.

Subsequent efforts further strengthened the use of this methodology, including studies validating both the BBB permeability to brain EVs (Dickens et al., 2017; Rufino-Ramos et al., 2022) and the enrichment of EV and neuronal markers in protein lysates of L1CAM IP eluates from human blood (Blommer et al., 2023; Fu et al., 2020; Jiang et al., 2020; Kapogiannis et al., 2019; Mustapic et al., 2017; Niu et al., 2020; Nogueras-Ortiz et al., 2020; Pulliam et al., 2019; Pulliam et al., 2020; Vreones et al., 2023). Additional observations supporting the suitability of the L1CAM IP for the isolation of brain NDEVs from blood include: 1) the recovery of GFP-positive EVs from the plasma of Nestin-GFP mice selectively expressing GFP in neurons (Mustapic et al., 2017); 2) positive correlations between brain and NDEV levels of pathological proteins in multiple AD mouse models (Delgado-Peraza et al., 2021); and 3) proteomic analyses detecting L1CAM in EVs isolated from human brains (Vella et al., 2017; You et al., 2022) and showing that a high percentage of proteins carried by EVs isolated from human blood via L1CAM IP are highly expressed in the human brain and shared with EVs isolated from the conditioned media of human neurons in culture (Anastasi et al., 2021; Pulliam et al., 2019).

Despite this cumulative evidence, the utility of L1CAM as a constituent of brain NDEVs in blood is still under debate due to potential limitations raised in multiple occasions (Fowler, 2019; Gomes & Witwer, 2022; Hill, 2019; Norman et al., 2021). First, although L1CAM was originally described as a neuronal transmembrane protein directly regulating axon guidance in the brain (Kenwrick et al., 2000), it is also expressed at comparable RNA levels by neurons and Schwann cells of the peripheral nervous system, kidney tubule epithelia, and skin epithelial cells and melanocytes (https://www.proteinatlas.org/ENSG00000198910-

20013078, 2024, 6, Downloaded from https://isevjournals.onlinelibrary.wiley.com/doi/10.1002/jev2.12459 by National Health And Medical Research Council, Wiley Online Library on [05/06/2025]. See the Terms and Conditions (https://onlinelibrary.wiley.com/terms-and-conditions) on Wiley Online Library for rules of use; OA articles are governed by the applicable Creative Commons License

L1CAM/single+cell+type). Hence, it is hypothesised that EVs from these additional cell sources end up in the circulation and contaminate brain NDEVs upon L1CAM IP. Second, blood contains high levels of free L1CAM (https://www.proteinatlas.org/ENSG00000198910-L1CAM/blood+protein) thought to interfere with the L1CAM IP by either blocking the recovery of NDEVs upon binding to capture antibodies or mediating the recovery of non-neuronal EVs upon binding to the protein surface of redundant blood-borne EVs. Third, upon ligand binding, L1CAM extracellular peptides can be released from cells via membrane proximal cleavage by metalloproteinases (Maten et al., 2019; Mechtersheimer et al., 2001), a process that could deplete blood-borne NDEVs from the L1CAM extraluminal epitopes targeted during L1CAM IP. Even a claim that L1CAM-positive EVs do not exist in biofluids has been made, based on inferences from size exclusion chromatography of cerebrospinal fluid and plasma showing that most L1CAM co-elutes with soluble proteins instead of EVs (Norman et al., 2021). Yet, until now, experiments have not directly addressed these hypotheses, which admittedly pose a scientific challenge to proponents of L1CAM IP and require the use of arising techniques capable of detecting the physical association of L1CAM with single vesicles alongside canonical EV and neuronal protein markers.

Among such techniques, flow cytometry analysis (FCA) offers great advantages for addressing whether L1CAM is a marker of NDEVs in blood. This technique has been recently shown to resolve single brain- and plasma-derived EVs by detecting the fluorescence emission of labelled EVs in combination with their light scattering as an indicator of particle diameter (Gomes et al., 2023; Libregts et al., 2018). In the present study, we aimed to shed light on the L1CAM controversy using FCA to 1) assess the physical association of L1CAM with EVs in human blood, 2) quantify the percentage of L1CAM-positive EVs in human blood originating from neuronal and non-neuronal cells, 3) test the non-specific binding of free L1CAM in blood to the extraluminal surface of EVs and 4) determine the degree of enrichment of L1CAM-positive NDEVs achieved by L1CAM IP.

Additional techniques were employed to further evaluate the association of L1CAM with blood-borne NDEVs. These include the assessment of proteomics studies to predict the compartmentalization of L1CAM in EVs from human brains and blood, and novel assays using the Simoa® and Luminex® technologies as well as transmission electron and fluorescent confocal microscopy for the co-detection of L1CAM with neuronal markers in canonical EVs.

2 | METHODS

Given their extent, detailed Methods are provided as Supplemental Material.

3 | RESULTS

3.1 | EVs secreted by cultured neurons carry the ectodomain of L1CAM

The utility of L1CAM as a target for the immunocapture of intact NDEVs from biofluids depends on the compartmentalization of its ectodomain to the EV membrane, which could be prevented by the activity of membrane proteases known to cleave L1CAM upon binding to ligands on neighbouring cells during cell adhesion signalling (Mechtersheimer et al., 2001). Previous observations have shown the sorting of L1CAM from the plasma membrane to multivesicular bodies upon ligand binding (Lutz et al., 2012), as well as its detection in EVs secreted by mouse, rat and human cultured neurons by mass spectrometry and immunoblots of EV lysates (Anastasi et al., 2021; Faure et al., 2006; Lachenal et al., 2011; Norman et al., 2021; Vilcaes et al., 2021). Although these observations suggest that L1CAM is carried by NDEVs, evidence at the single-vesicle level validating the physical association of the L1CAM ectodomain with NDEVs is missing. We addressed this by evaluating the detection of extraluminal L1CAM epitopes in NDEVs via fluorescent confocal microscopy and nanoscale multiplex FCA.

We performed differential ultracentrifugation (UC) of conditioned media of rat cortical and human induced pluripotent stem cell-derived neuronal cultures (iNeurons) (Figure S1), isolating rat NDEVs and human iNDEVs, respectively (Figure 1a). NDEVs had an EV-typical size profile (50–500 nm) based on nanoparticle tracking analysis (NTA) results (Figure 1b) showing an EV yield of $5.9 \pm 0.3 \times 10^9$ particles/mL (mean ± standard deviation) for rat NDEVs and $8.4 \pm 0.6 \times 10^{10}$ particles/mL for iNDEVs that was not confounded by contaminating nanoparticles from the supplemented basal media (termed vehicle in Figure 1b) as these were undetected. NDEVs carried full-length L1CAM alongside neuronal (β-III-tubulin) and EV markers (Alix, Flotillin-1 and CD81) as illustrated by immunoblots (Figure 1c) also showing the absence of the non-exosomal Golgi marker GM130 confirming that NDEV preparations were devoid of intracellular nanoparticles that could be co-isolated along EVs if the conditioned media is collected under cytotoxic conditions. Using fluorescent confocal microscopy and antibodies EPR18750 and 5G3 targeting the L1CAM ectodomain (Figure S2), we detected single NDEVs carrying L1CAM co-localised with multiple EV markers (Figure 1d,e). The association of the L1CAM ectodomain with NDEVs was confirmed using FCA capable of detecting single membranous nanoparticles by combining violet side scatter (vSSC), an indicator of particle size, with fluorescence-based particle detection (Figure S3) under non-swarming conditions to avoid the coincidence of events (Figure S4). FCA of EVs gated based on the detection of blue fluorescent succinimidyl ester (BSE) staining all EVs (Morales-Kastresana et al., 2017) (Figure 1h,l) revealed that a

20013078, 2024, 6, Downloaded from https://isevjournals.onlinelibrary.wiley.com/doi/10.1002/jev2.12459 by National Health And Medical Research Council, Wiley Online Library on [05/06/2025]. See the Terms and Conditions (https://onlinelibrary.wiley.com/terms-and-conditions) on Wiley Online Library for rules of use; OA articles are governed by the applicable Creative Commons License

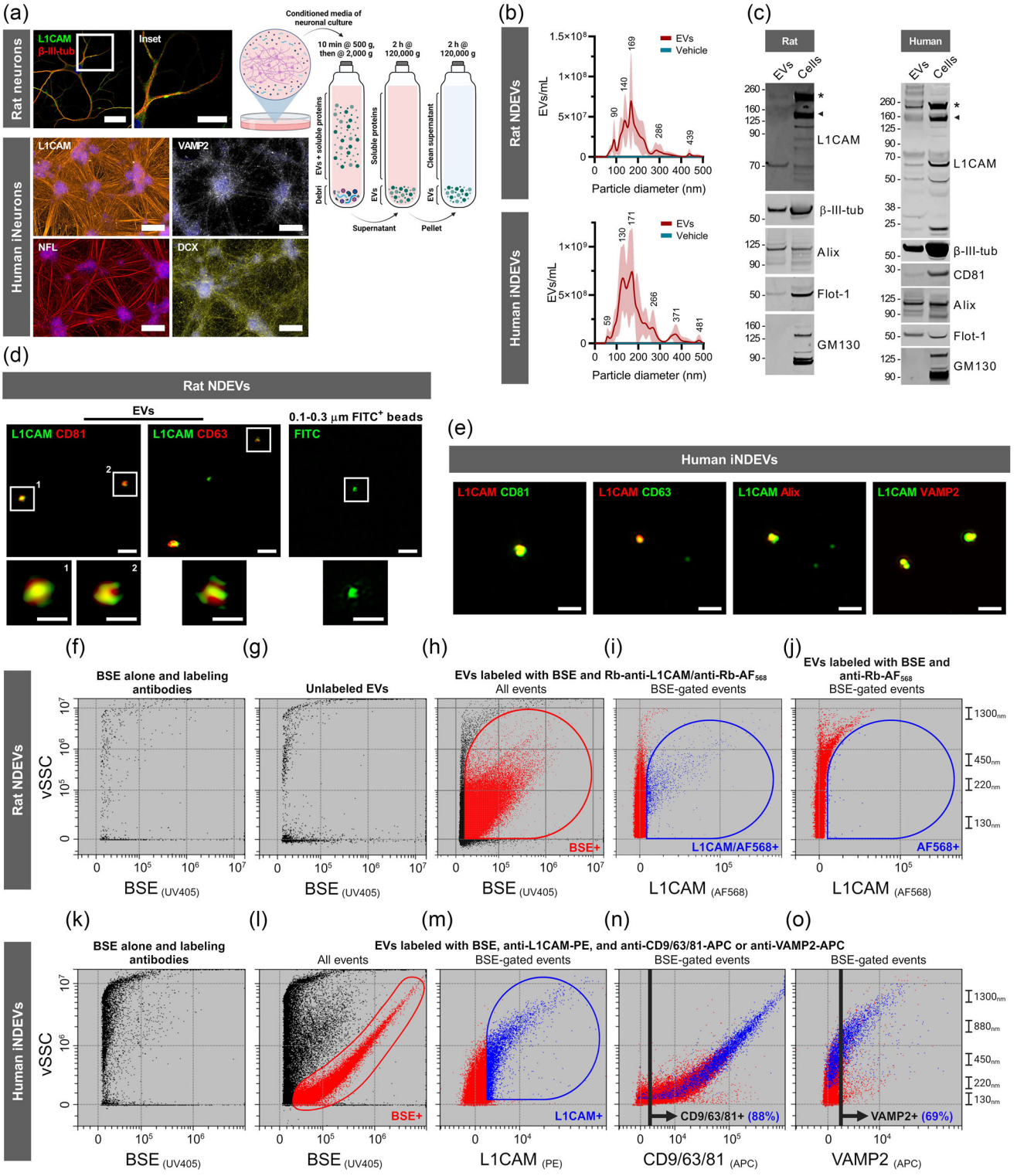

FIGURE 1 High-resolution fluorescent confocal microscopy and nanoscale multiplex flow cytometry analysis detect L1CAM in single neuron-derived EVs. (a) Diagram of the differential ultracentrifugation methodology used for the isolation of EVs from the conditioned media of rat hippocampal neurons and human iNeurons (namely, rat NDEVS and human iNDEVs, respectively) (created with BioRender; agreement number: MF23W0TRTS). The expression of L1CAM and additional neuronal markers in cultured neurons is demonstrated by immunocytochemistry (nuclei visualised using DAPI in blue; scale bars: 20 μm; scale bar of box inset: 10 μm). (b) Histogram of EV concentration as function of particle diameter from nanoparticle tracking analysis (NTA) of rat NDEVs, human iNDEVs and their respective vehicles (cell media subjected to the same EV isolation methods). (c) Immunoblots of rat and human EV and neuronal lysates showing the expression of full-length L1CAM (asterisk) and products of lower molecular weight (arrowhead) (using anti-L1CAM antibody clone EPR18750 under reducing conditions; Figure S2), as well as canonical neuronal (β-III-tubulin) and EV (CD81, Alix and Flotillin-1) markers. (d and e)

(Continues)

20013078, 2024, 6, Downloaded from https://isevjournals.onlinelibrary.wiley.com/doi/10.1002/jev2.12459 by National Health And Medical Research Council, Wiley Online Library on [05/06/2025]. See the Terms and Conditions (https://onlinelibrary.wiley.com/terms-and-conditions) on Wiley Online Library for rules of use; OA articles are governed by the applicable Creative Commons License

FIGURE 1 (Continued)

High resolution fluorescent confocal microscopy of rat NDEVs (d) and human iNDEVs (e) showing the co-immunolabelling of L1CAM and EV markers in single particles with nano-scale sizes confirmed by the detection of FITC-positive beads with sizes ranging from 100 to 300 nm (scale bars: 500 nm). Images of selected nanoparticles were captured at a higher magnification and are shown in box insets (scale bars: 200 nm). High-sensitivity nanoscale multiplex flow cytometry analysis (FCA) (f–o). Dot plots show the violet size scatter (vSSC) in function of the fluorescent signal of rat (f–j) and human (k–o) NDEV samples co-labelled with the fluorescent EV marker BSE (h and l) and fluorescent antibodies against L1CAM (i and m). Human iNDEVs were also labelled with fluorescent antibodies against either tetraspanins (n) or VAMP2 (o). Gates enclosing events positive for a given marker were designated based on the background signal of negative controls (f, g and k). The frequency of events (events/sec) in analysed samples did not result in coinciding events as confirmed by swarming experiments (Figure S4a,b). Dot plots (n) and (o) include the percentage of L1CAM-positive events double-positive for tetraspanins and VAMP2. A size range based on the vSSC of FITC-tagged beads (Figure S3) is included on the right of each panel for the size comparison of events.

vast subpopulation of L1CAM+ nanoparticles (Figure 1i,m) from iNeurons are double positive for pan-tetraspanins (Figure 1n; 97.01 ± 0.02%, mean ± standard deviation), also carrying the synaptic EV protein VAMP2 (Vilcaes et al., 2021) (Figure 1o, You et al., 2022). These findings validate the sorting of L1CAM extraluminal epitopes to NDEVs and demonstrate the ability of fluorescent confocal microscopy and FCA to examine the existence of L1CAM+ NDEVs in human blood at the single-vesicle level.

3.2 | L1CAM is associated with the extraluminal surface of blood-borne EVs

Next, we interrogated the preservation of the L1CAM ectodomain targeted during L1CAM IP in EVs isolated from human blood. We hypothesised that L1CAM is mostly present in larger plasma EVs, since L1CAM+ iNDEVs were predominantly sedimented at 10,000 × *g* (10K) compared to the 120,000 × *g* (120K) pellet (Figure S5g,h,k vs. i,j,l and m) containing smaller particles (ExoView™: 79.4 ± 9.3 vs. 73.4 ± 10.7 nm, mean ± standard deviation of CD9, CD63 and CD81+ EVs; NTA: 221.4 ± 9.2 vs. 163.0 ± 3.7 nm, mean ± standard error; Figure S5c–f). Hence, we fractionated the plasma from three human subjects in 13 fractions using a solid phase with a 70 nm pore size with the goal of purifying larger EVs in early SEC fractions from EVs smaller than 70 nm expected to co-elute with free proteins in later fractions.

The yield, size, and purity of nanoparticles was determined by analysing the collected fractions via FCA of BSE+ events, interferometry nanoparticle analysis by ExoView™, and assays to quantify free plasma proteins. FCA showed that the majority of BSE+ nanoparticles eluted in fractions 1–6 (82 ± 13% out of the sum total of BSE+ events in all fractions equivalent to $1.5 \pm 0.8 \times 10^7$ particles/mL; mean ± standard deviation), whereas less events were detected in later SEC fractions 7–13 (18 ± 13% equivalent to $3.1 \pm 3.4 \times 10^6$ particles/mL; mean ± standard deviation) (Figures 2a and S6). We assessed if our SEC methodology separated EVs based on their size using ExoView™ for the detection of the interferometry signals from tetraspanin+ nanoparticles that were immobilised in microchip spots individually coated with anti-CD9, -CD63 and -CD81 antibodies (Figure 2b,c). ExoView™ analyses of SEC fractions 1, 4, 7, 10 and 13 showed that in parallel with plasma fractionation, there was a gradual decrease in the size of CD9+, CD63+ and CD81+ EVs (Figure 2c; 67.1 ± 5.5 nm mean EV size in fraction 4 compared to 59.8 ± 1.1 nm in fraction 10; mean ± standard deviation). EV yield also decreased in parallel with plasma fractionation in line with FCA observations and confirming that most EVs eluted in early SEC fractions (Figure 2b; 1,095.1 ± 192.5, 307.8 ± 39.8, and 278.3 ± 136.6 mean number of CD9+, CD63+ and CD81+ particles, respectively, in SEC fraction 4 compared to 308.0 ± 126.9, 153.7 ± 19.6, and 81.1 ± 5.5 in fraction 10; error: standard deviation). Finally, we assessed the purification of larger EVs in early SEC fractions from free plasma proteins by measuring the fractionation of total protein and albumin, one of the most abundant free proteins in human blood plasma. Equal parts of intact SEC fractions were subjected to the BCA total protein assay and an albumin ELISA, with results showing a gradual increase of total protein and albumin in parallel with plasma fractionation (Figure 2a). For the albumin ELISA, the signal became detectable in fraction 7 and peaked in fractions 10–12 depending on the subject, suggesting that EVs predominantly eluting in early SEC fractions 1–6 are purified from free plasma proteins. On the other hand, the BCA signal peaked earlier in fractions 8–10 and became detectable in fraction 4 most probably due to external protein epitopes carried by nanoparticles predominantly eluting in this fraction based on FCA results. Based on these results, we considered SEC fractions 1–5 as EV fractions to account for the potential contamination of EVs in SEC fraction 6 with small amounts of free plasma proteins.

The association of L1CAM with SEC fractions was assessed using a previously described Simoa® assay for the non-selective detection of EV-associated and soluble L1CAM using capture and detection antibodies targeting two different epitopes of the L1CAM ectodomain (Norman et al., 2021) (Figure 2d; Figure S2a illustrates epitopes targeted by L1CAM antibodies). We observed that most L1CAM in plasma was detected in SEC fractions 6–13, with lower concentrations above the assay's lower limit of quantification (LLoQ) in SEC fractions 1 to 5 (Figure 2e; Figure S7a,b). Since the L1CAM/L1CAM Simoa® cannot distinguish between soluble and EV-associated L1CAM, we developed an L1CAM/pan-tetraspanin Simoa® assay for the detection of the L1CAM ectodomain only on intact EVs co-carrying the canonical EV markers CD9, CD63 and CD81 which are members of the tetraspanin family (Figure 2d). This assay revealed the presence of EV-associated L1CAM in both early and late SEC fractions

20013078, 2024, 6, Downloaded from https://isevjournals.onlinelibrary.wiley.com/doi/10.1002/jev2.12459 by National Health And Medical Research Council, Wiley Online Library on [05/06/2025]. See the Terms and Conditions (https://onlinelibrary.wiley.com/terms-and-conditions) on Wiley Online Library for rules of use; OA articles are governed by the applicable Creative Commons License

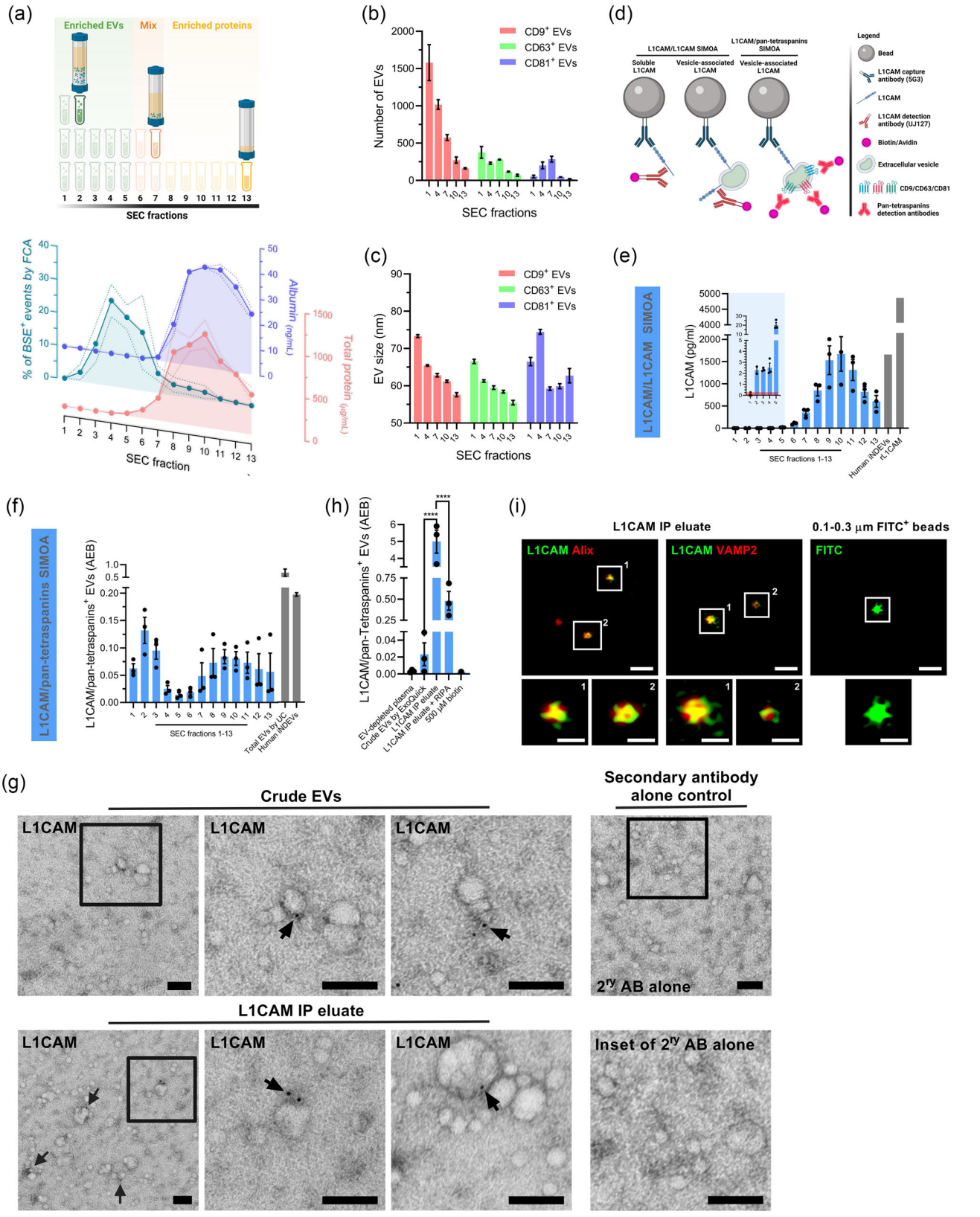

FIGURE 2 Detection of EV-associated L1CAM in human plasma. On the top of (a), a diagram (created with BioRender; agreement number: JD23W0UDJ4) illustrates the (partial) separation of EVs and soluble proteins from plasma using size exclusion chromatography (SEC). SEC performance was corroborated by the quantification of EVs and soluble plasma proteins in collected fractions using FCA of BSE+ EVs, BCA total protein assay, albumin ELISA (bottom panel in a) and interferometry nanoparticle analysis by ExoView® (b and c). In (b) and (c), bar graphs show the number and size of tetraspanin-positive EVs (based on the interferometry signal of particles captured by anti-CD9, -CD63 or -CD81 antibodies) in equal volumes of SEC fractions.

(Continues)

20013078, 2024, 6, Downloaded from https://isevjournals.onlinelibrary.wiley.com/doi/10.1002/jev2.12459 by National Health And Medical Research Council, Wiley Online Library on [05/06/2025]. See the Terms and Conditions (https://onlinelibrary.wiley.com/terms-and-conditions) on Wiley Online Library for rules of use; OA articles are governed by the applicable Creative Commons License

FIGURE 2 (Continued)

The signal from particles captured with an isotype control (mIgG) was subtracted from that of tetraspanin+ particles to account for the non-specific binding of EVs to the ExoView® chip. (d), Simoa® assays for the detection of L1CAM in EVs from blood are illustrated (created with BioRender; agreement number: EN23W0UMNQ). In (e) and (f), bar graphs show the mean protein concentration of L1CAM or the average enzymes per bead (AEB) signal of L1CAM+ EVs as measured by L1CAM/L1CAM or L1CAM/pan-tetraspanins Simoa® assays, respectively. An inset in the L1CAM/L1CAM Simoa® graph shows results with an adjusted y-axis including the assay's LLoQ in red. Recombinant human L1CAM, iNDEVs and plasma EVs isolated by ultracentrifugation at 120,000 × *g* were used as positive controls. (g) Immuno-TEM images showing the deposition of anti-L1CAM antibody clone 5G3 (arrows) in nanoparticles from plasma (pooled SEC fractions 1–5) before (crude EVs) and after (eluate) L1CAM IP. For images of 'Crude EVs' and 'L1CAM IP eluate' samples showing L1CAM immunoreactivity, box insets on widefield images on the far left enclose the areas magnified in the centre panels which are followed by images on the right corresponding to replicate TEM images of the same samples. Images of the 'L1CAM IP eluate' sample incubated with secondary antibody (2^{ry} AB) alone on the far right assess non-specific binding. Scale bars, 100 nm. (h) A bar graph of the AEB signal from the L1CAM/pan-tetraspanins Simoa® of EVs isolated from plasma via ExoQuick® sedimentation before (crude EVs) and after (eluate) L1CAM IP. The low signal obtained by the supernatant collected after sedimentation of EVs (EV-depleted plasma) suggests the EV-specificity of the L1CAM/pan-tetraspanins Simoa® assay. The abolition of the signal with treatment of the L1CAM IP eluate with RIPA detergent further confirms the specificity of the signal for membrane enclosed tetraspanin+ particles. The AEB from free biotin accounts for the non-specific signal of biotinylated IP antibodies in the L1CAM IP eluate. Statistical analysis: two-way ANOVA; $^{****}p < 0.0001$. (i) High resolution fluorescent confocal microscopy of the L1CAM IP eluate showing the co-immunolabelling of L1CAM and EV markers in single particles with nano-scale sizes confirmed by the detection of FITC-positive beads with sizes ranging from 100 to 300 nm (scale bars: 500 nm). Selected nanoparticles enclosed by box insets were captured at a higher magnification (scale bars: 200 nm). Graphs a–f and h average sample replicates from three different subjects. All experiments were repeated at least once using samples from additional donors with similar results.

(Figure 2f; Figure S7c,d), as well as in plasma EVs sedimented at both 10 and 120K (Figure S8a–c), suggesting that, in blood, both large and small EVs carry extraluminal L1CAM accessible for immunocapture. Consistently, the L1CAM/pan-tetraspanin Simoa® assay showed that performing L1CAM IP in crude EVs isolated from plasma via ExoQuick® sedimentation results in many-fold increase of detergent-sensitive L1CAM+ nanoparticles (Figure 2h). The association of the L1CAM ectodomain with plasma EVs was further confirmed by transmission electron microscopy and confocal microscopy of pooled SEC fractions 1–5 (NTA and Cryo-TEM characterization shown in Figure S9) before and after L1CAM IP (Figure 2g,i).

3.3 | Identification of the L1CAM ectodomain in brain- and blood-derived EVs by mass spectrometry

Multiple proteomic studies have identified L1CAM in EVs isolated from human brains and blood in association with canonical EV and neuronal markers, providing L1CAM as a suitable target for the affinity immunocapture of circulating NDEVs (Anastasi et al., 2021; Vassileff et al., 2020; You et al., 2023). However, the identity of the L1CAM peptides was not disclosed, thus leaving unaddressed the hypothesis that circulating NDEVs might carry L1CAM products of membrane proximal proteolysis devoid of the ectodomain targeted via L1CAM IP. We tested this hypothesis by performing *a posteriori* mass spectrometry bioinformatics to reveal the L1CAM domains carried by brain- and blood-derived NDEVs. Our analysis identified peptides corresponding to the L1CAM ectodomain in three independent proteomic datasets of highly purified small EVs isolated from post-mortem human brain tissue via density gradient and plasma-derived EVs subjected to L1CAM IP (Table 1). Of note, multiple peptides spanned the immunoglobin-like domains (Ig) 2 and 3 and the fibronectin-type III (FNIII) repeat 4 (Table 1, in bold) targeted by the L1CAM antibody clones 5G3 and UJ127 commonly used for the immunocapture of NDEVs (Figure S2a). Interestingly, the same peptide was identified in all three mass spectrometry datasets (Table 1, in bold), consisting of amino acids 604–617 spanning the binding site of the protease ADAM10 which is one of the main catalysers of L1CAM membrane shedding (Linneberg et al., 2019). These results strengthen the hypothesis that brain- and blood-derived NDEVs carry uncleaved extraluminal L1CAM accessible for affinity immunocapture.

3.4 | Soluble L1CAM in blood does not bind to the surface of EVs

It has been hypothesised that soluble L1CAM in plasma mainly originates via proximal membrane cleavage in L1CAM-expressing peripheral organ cells, releasing multiple L1CAM peptides of variable molecular weight that could 'escape' adsorption to the extracellular matrix and, consequently, not participate in cell adhesion signalling (Maten et al., 2019; Mechtersheimer et al., 2001). High concentrations of extracellular L1CAM peptides in plasma represent a potential confounding factor in L1CAM EV-related studies, as L1CAM+ EVs could originate from the binding of soluble L1CAM to the protein corona of various blood-borne EVs. A previous profiling of the protein corona of plasma EVs is reassuring in that regard, as L1CAM was not detected (Toth et al., 2021). Nevertheless, we sought to test it directly by first, incubating L1CAM-negative EVs isolated from the conditioned media of HEK cells, known to not express L1CAM, with soluble proteins from human plasma, and then using FCA to assess the adsorption of L1CAM to the surface of intact EVs, as well as that of ApoA1 (Figure 3a), a main constituent of the protein corona of plasma EVs (Toth et al., 2021).

20013078, 2024, 6, Downloaded from https://isevjournals.onlinelibrary.wiley.com/doi/10.1002/jev2.12459 by National Health And Medical Research Council, Wiley Online Library on [05/06/2025]. See the Terms and Conditions (https://onlinelibrary.wiley.com/terms-and-conditions) on Wiley Online Library for rules of use; OA articles are governed by the applicable Creative Commons License

TABLE 1 Identification of the L1CAM ectodomain in brain- and blood-derived EVs by independent proteomic studies.

			Extracellular L1CAM peptides identified			
Study	**EV source**	**EV isolation method**	*Sequence*	*Range of residues*	*Ectodomains spanned by identified peptides*	**Notes**
You et al. (2023); Toth et al. (2021)	Human brain tissue ($N = 3$)	Density gradient fraction corresponding to small EVs subjected to ATP1A3 immunocapture	***AQLLVVGSPGPVPR***	604-617	Ig6/FNIII-1	Peptide identified in all EV samples prior to IP and 2/3 IP eluates
Vassileff et al. (2020); Linneberg et al. (2019)	Human brain tissue ($N = 11$)	Density gradient fraction corresponding to small EVs	AFGAPVPSVQWLDEDGTTVLQDER	450-473	Ig5	16/20 peptides identified in EV samples also detected in source brain protein lysates
			AQLLVVGSPGPVPR	604-617	Ig6/FNIII-1	
			ETVKPVEVEEGESVVLPCNPPPSAEPLR	141-168	***Ig2 (5G3)***	
			GALILSNVQPSDTMVTQCEAR	387-407	Ig4	
			GQLSFNLRDPELR	964-976	***FNIII-4 (UJ127)***	
			HAYYVTVEAAPYWLHKPQSHLYGPGETAR	323-351	Ig3/Ig4	
			HGLLLANAYIYVVQLPAK	410-427	Ig4-Ig5	
			INGIPVEELAK	368-378	Ig4	
			INGIPVEELAKDQK	368-381	Ig4	
			LDCQVQGRPQPEVTWR	352-367	Ig4	
			LVLSDLHLLTQSQVR	618-632	FNIII-1	
			NRHGLLLANAYIYVVQLPAK	408-427	Ig4-Ig5	
			TIIQKEPIDLR	218-228	***Ig2-Ig3 (5G3)***	
			VSWSPAEDHNAPIEK	633-647	FNIII-1	
			VSWSPAEDHNAPIEKYDIEFEDKEMAPEK	633-661	FNIII-1	
			VTFTCQASFDPSLQPSITWR	535-554	Ig6	
			WLRPSGPMPADR	276-287	Ig3	
			WQPPLSHNGVLTGYVLSYHPLDEGGKGQLSFNLRDPELR	938-976	***FNIII-4 (UJ127)***	
			WRPVDLAQVK	833-842	FNIII-3	
			YDIEFEDKEMAPEK	648-661	FNIII-1	
Anastasi et al. (2021); Hill (2019)	Plasma ($N = 4$)	Plasma pre-cleared at 10,000 × *g* subjected to L1CAM immunocapture using the UJ127 antibody	***AQLLVVGSPGPVPR***	604-617	Ig6/FNIII-1	Peptide identified in EV samples from 2/4 subjects

20013078, 2024, 6, Downloaded from https://isevjournals.onlinelibrary.wiley.com/doi/10.1002/jev2.12459 by National Health And Medical Research Council, Wiley Online Library on [05/06/2025]. See the Terms and Conditions (https://onlinelibrary.wiley.com/terms-and-conditions) on Wiley Online Library for rules of use; OA articles are governed by the applicable Creative Commons License

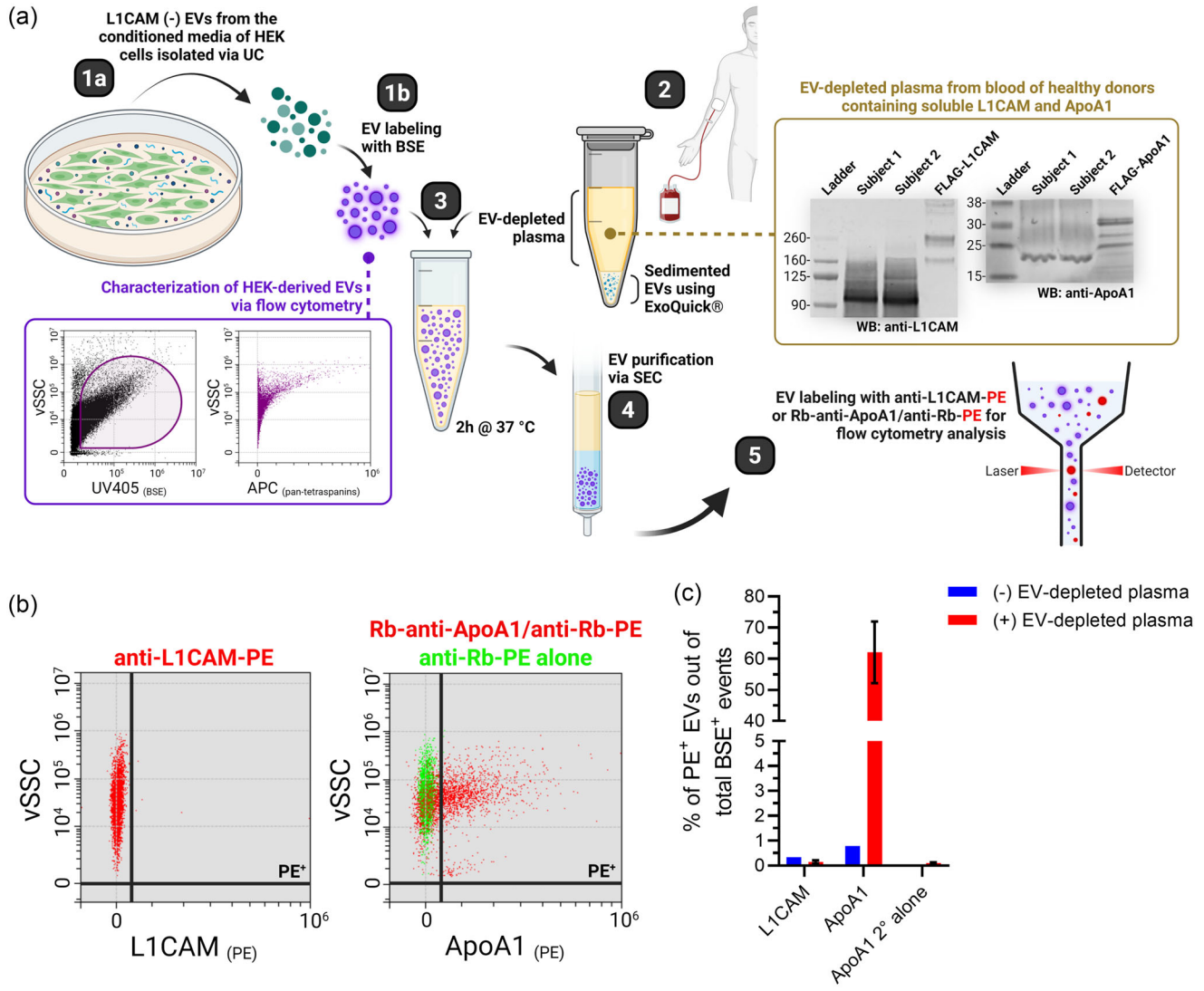

FIGURE 3 Soluble L1CAM in blood does not binds to the surface of EVs. (a) A diagram (created with BioRender; agreement number: LX25DH5BU3) of the methodology followed to assess the binding of soluble L1CAM and ApoA1 in plasma to the surface of EVs in vitro. L1CAM-negative EVs were isolated from the conditioned media of HEK-293 cells, that naturally do not express L1CAM, via ultracentrifugation at 120,000 x g (step 1a) and labelled with the total EV marker BSE (step 1b). Flow cytometry analysis (FCA) confirmed the BSE labelling (vSSC vs. BSE dot plot on the left) and EV origin (vSSC vs. APC-CD9/CD63/CD81 signal of BSE-gated events on the right) of HEK-derived EVs. Then, BSE-labelled EVs were incubated with soluble plasma proteins from two human subjects separately (step 3), depleted of EVs by ExoQuick® sedimentation (step 2), consisting of L1CAM and ApoA1 as confirmed by immunoblots (using L1CAM antibody clone EPR18750 targeting the ectodomain; refer to Figure S2 for target epitope). After incubation, BSE-labelled EVs were purified from soluble plasma proteins by size exclusion chromatography (step 4) and subjected to fluorescent labelling with PE-tagged anti-L1CAM antibody (5G3 clone) or rabbit anti-ApoA1 plus PE-tagged anti-rabbit antibodies for FCA (step 5). (b) Dot plots showing the vSSC versus PE signal of BSE-gated events identified by FCA of BSE+ HEK-derived EVs incubated with soluble plasma proteins from a human subject and labelled either with PE-tagged anti-L1CAM (red events, left), rabbit anti-ApoA1 plus PE-tagged anti-rabbit antibodies (red events, right), or PE-tagged anti-rabbit antibody alone (green events, right). A PE gate designated based on the background signal of negative controls (unlabelled EVs and EVs labelled with secondary antibody) encloses events positive for L1CAM (left) or ApoA1 (right). (c) A bar graph indicates the mean percentage with standard error of HEK-derived EVs positive for L1CAM or ApoA1 (PE gated) out of total EVs (BSE+ events), after incubation with soluble plasma proteins (red bars) or left untreated (blue bars). Error bars represent the standard error of the mean from values of EVs incubated with soluble plasma proteins from two human subjects.

First, we validated the EV identity of BSE-labelled HEK-derived nanoparticles via FCA detecting a high abundance of BSE-gated nanoparticles positive for pan-tetraspanins CD9, CD63 and CD81 (Figure 3a, step 1b). In parallel, we used immunoblotting to confirm the presence of soluble L1CAM and ApoA1 in human plasma depleted from EVs via ExoQuick® sedimentation (Figure 3a, step 2). Immunoblotting using the L1CAM antibody clone EPR18750 targeting the ectodomain (Figure S2a,b) showed that most of soluble L1CAM in plasma is proteolytically cleaved with a small fraction migrating between the 260 and 160 kDa protein ladder standards and close to the molecular weight of full length L1CAM reported to be 220 kDa (Figure 3a, step 2). FCA showed that BSE-gated HEK-derived EVs positive for L1CAM and ApoA1 are barely detectable (Figure 3c), and that upon incubation with soluble plasma proteins, only ApoA1+ EVs are drastically increased (from 0.79 to 62.1 ± 14.1), whilst levels of

20013078, 2024, 6, Downloaded from https://isevjournals.onlinelibrary.wiley.com/doi/10.1002/jev2.12459 by National Health And Medical Research Council, Wiley Online Library on [05/06/2025]. See the Terms and Conditions (https://onlinelibrary.wiley.com/terms-and-conditions) on Wiley Online Library for rules of use; OA articles are governed by the applicable Creative Commons License

L1CAM+ EVs remained unchanged (from 0.3 to 0.2 ± 0.1) (Figure 3b,c). These results suggest that soluble L1CAM in plasma does not bind to the protein corona of plasma EVs and that L1CAM+ blood-borne EVs carry the L1CAM ectodomain from the cell of origin.

3.5 | Quantification of L1CAM+ EVs of neuronal origin in human blood

We leveraged the multiplex detection capabilities of FCA at the single-EV level to assess the neuronal origin of L1CAM+ EVs in blood by quantifying the abundance of EVs co-carrying L1CAM with canonical neuronal markers among total plasma EVs isolated via UC directly at 120K (Figure 1a) resulting in the sedimentation of both large and small EVs. FCA of BSE-gated events with scattering and fluorescent signals distinct from background noise and within the range of fluorescent nanobeads 130–880 nm in size (Figure 4a,b) revealed that 3.8 ± 0.9 % of plasma EVs carry L1CAM (Figure 4c–e), 43.3 ± 5.5% pan-tetraspanins (Figure 4f,g), 5.0 ± 1.9% VAMP2 (Figure 4i,j) and 4.14 ± 1.08% β-III-tubulin (Figure 4l,m) (mean ± standard deviation). The sensitivity of BSE-gated nanoparticles to detergent treatment confirmed the membrane composition of L1CAM+ events (Figure 4a). The EV and neuronal origins of partially permeabilised L1CAM+ nanoparticles were assessed by co-labelling with tetraspanin membrane EV markers (Figure 4f–h), or the membrane and cytoplasmic neuronal proteins VAMP2 (Figure 4i–k) and β-III-tubulin (Figure 4l–n; refer to Figure S10 for the validation of intraluminal FCA under partial membrane permeabilization), respectively. Quantification of double-positive BSE-gated events indicates that, in human blood, 67.4 ± 5.6 % of L1CAM+ EVs carry at least one of the canonical tetraspanins, 33.6 ± 3.6% carry VAMP2, and 54.0 ± 8.5% carry β-III-tubulin (Figure 4o). In contrast, only 2.38 ± 1.51% of L1CAM-negative (L1CAM-) EVs were positive for VAMP2 and 1.30 ± 0.46% for β-III-tubulin (Figure S11). The percentages of L1CAM+ EVs double-positive for all the markers evaluated as part of the experiment shown in Figure 4, out of all BSE events, were as follows (mean ± standard deviation): L1CAM/pan-tetraspanin++ EVs, 2.49 ± 0.37%; L1CAM/VAMP2++ EVs, 1.26 ± 0.29%; L1CAM/β-III-tubulin++ EVs: 2.06 ± 0.63%. Similar results were obtained in plasma EVs isolated by SEC (data not shown). The presence of both large and small L1CAM+ NDEVs in human blood was confirmed by flow cytometry of plasma EVs sedimented at 10 and 120 K, respectively, detecting L1CAM/β-III-tubulin double positive events in both fractions (Figure S8d). The association of L1CAM with NDEVs in blood was further confirmed by confocal microscopy of plasma EVs recovered via L1CAM IP, showing single nanoparticles double positive for L1CAM and VAMP2 (Figure 2i).

3.6 | Enrichment of L1CAM+ NDEVs via L1CAM IP of human plasma

The relatively low concentration of NDEVs in blood—defined here as EVs positive for the neuronal and synaptic markers β-III-tubulin and VAMP2, respectively—carrying the L1CAM ectodomain, as shown in Figures 2 and 4, reinforces the need for enrichment of L1CAM+ EVs for downstream biomarker studies. Numerous reports by different groups concur on the utility of L1CAM as a target for the enrichment of NDEVs (Gomes & Witwer, 2022; Vandendriessche et al., 2022), showing that L1CAM IP of blood-borne EVs results in the enrichment of neuronal and preservation of EV markers, as well as the enrichment of protein biomarkers for brain diseases. However, there is still controversy about the interpretation of these results as 1) most observations have been made using immunoblots and protein assays with signals that could arise from EV-associated proteins or soluble confounding factors alike, and 2) the specificity of IP targeting extracellular L1CAM epitopes towards plasma NDEVs could be reduced by L1CAM+ EVs originating from non-neuronal cells and free forms of the L1CAM ectodomain. We addressed these limitations using FCA to quantify the proportion of single NDEVs before and after L1CAM IP of total plasma EVs.

FCA of BSE-gated plasma EVs with scattering and fluorescent signals distinct from background noise (Figure 5a,c) revealed that IP of SEC-isolated plasma EVs targeting the L1CAM ectodomain with the antibody clone 5G3 results in a ~24-fold enrichment of L1CAM+ EVs over plasma EVs and EVs immunoprecipitated with an isotype control antibody (Figure 5b vs. d, f and g; Figure S12a). A high percentage of immunocaptured L1CAM+ EVs carried tetraspanins and VAMP2, whilst being negative for ASGR2, a membrane marker of hepatocytes considered a main source of peripheral L1CAM (Ghosh et al., 2020) (Figure 5h–k), thus confirming the EV identity and neuronal origin of a sizable sub-population of L1CAM+ EVs recovered via L1CAM IP. Following L1CAM IP, the percentages of L1CAM+ EVs double-positive for all the markers evaluated as part of the experiment shown in Figure 5, out of all BSE events, were as follows (mean ± standard deviation): L1CAM/pan-tetraspanin++ EVs, 50.09 ± 13.51%; L1CAM/VAMP2++ EVs, 37.47 ± 10.11%; L1CAM/ASGR2++ EVs, 0.30 ± 0.05%.

We calculated the concentration of L1CAM/VAMP2++ events shown in Figures 4 and 5 and compared the yield of this NDEV subpopulation in common between the two independent sets of experiments to evaluate 1) the reproducibility of both our crude EV isolation methodology and FCA, and 2) the degree of enrichment of L1CAM+ NDEVs from plasma achieved via L1CAM IP. The values that were used to calculate the average concentration of L1CAM/VAMP2++ events per millilitre of samples analysed in Figure 4 (crude EVs) and 5 (crude EVs and L1CAM IP eluate) were the following: FCA flow rate (10 µL/min), time of sample analysis, sample dilution, total BSE events, percentage of L1CAM/VAMP2++ events out of total BSE events and sample volume. Results were as follows (mean ± standard deviation): 6.75 ± 1.13 × 10^3 events per millilitre of crude EVs in Figure 4;

20013078, 2024, 6, Downloaded from https://isevjournals.onlinelibrary.wiley.com/doi/10.1002/jev2.12459 by National Health And Medical Research Council, Wiley Online Library on [05/06/2025]. See the Terms and Conditions (https://onlinelibrary.wiley.com/terms-and-conditions) on Wiley Online Library for rules of use; OA articles are governed by the applicable Creative Commons License

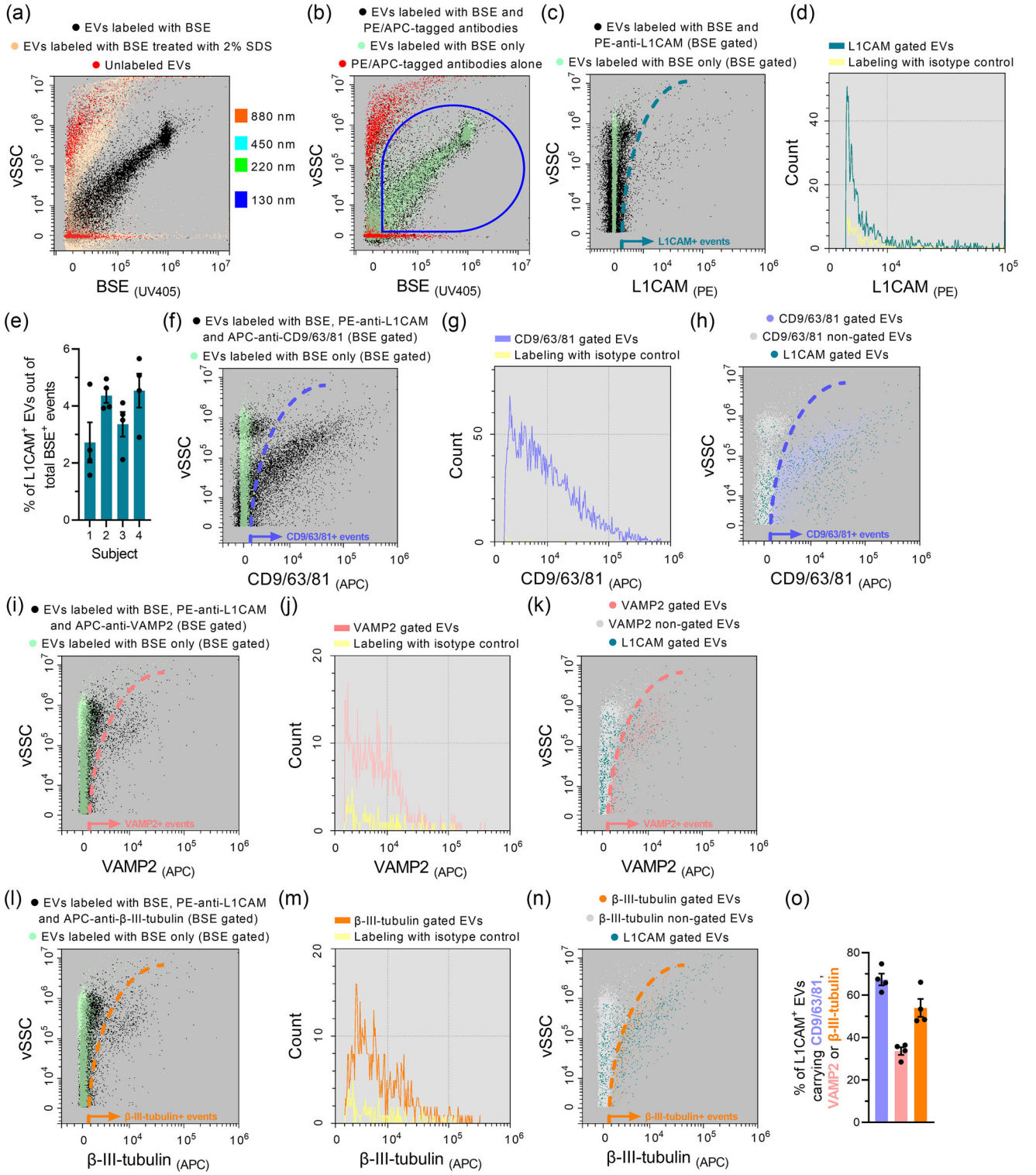

FIGURE 4 Quantification of the percentage of L1CAM+ EVs in human plasma carrying canonical EV and neuronal markers. Flow cytometry analysis of crude EVs isolated from human plasma via ultracentrifugation (UC) at 120,000 × *g* and triple-labelled with the fluorescent EV marker BSE, PE-tagged anti-L1CAM antibody (5G3 clone) and APC-tagged antibodies targeting either pan-tetraspanins (a cocktail of anti-CD9, -CD63 and -CD81 antibodies), VAMP2 or *β*-III-tubulin. In (a) a dot plot shows the vSSC in function of the BSE fluorescent signal in crude plasma EVs from a human subject, either unlabelled (red events) or labelled with BSE before (black events) and after (beige events) treatment with 2% SDS. A colour-coded size range based on the vSSC of FITC-tagged beads (Figure S3) is included on the right for the size comparison of events. In (b) a dot plot overlays the vSSC versus BSE signal of PE- and APC-tagged antibodies alone in PBS-1X (red events), and crude plasma EVs from the same human subject as in (a), labelled either with BSE plus PE- and APC-tagged antibodies (black events) or BSE only (light green events). A blue gate designated based on the background signal of negative controls (unlabelled

(Continues)

20013078, 2024, 6, Downloaded from https://isevjournals.onlinelibrary.wiley.com/doi/10.1002/jev2.12459 by National Health And Medical Research Council, Wiley Online Library on [05/06/2025]. See the Terms and Conditions (https://onlinelibrary.wiley.com/terms-and-conditions) on Wiley Online Library for rules of use; OA articles are governed by the applicable Creative Commons License

FIGURE 4 (Continued)

EVs as well as PE- and APC-tagged antibodies without EVs) encloses events positive for BSE. In (c) a dot plot overlays the vSSC versus PE signal of BSE-gated events in crude plasma EVs from the same human subject as in (a) and (b) labelled either with BSE plus PE-tagged anti-L1CAM antibody (5G3 clone) (black events) or BSE only (light green events). A turquoise dashed line designated based on the background signal of negative controls (unlabelled EVs, EVs labelled with a PE-tagged isotype control antibody, and PE-tagged anti-L1CAM antibody alone) gates events positive for L1CAM (events laying on the right of the dashed line). In (d) a histogram shows the number of L1CAM-gated events in (c) (turquoise line) overlayed with results of EVs labelled with BSE plus PE-tagged isotype control antibody (yellow line). The frequency of events in analysed samples (157 ± 55 events/s; $n = 22$ samples) did not resulted in coinciding events as confirmed by swarming experiments (Figure S4c,d). In (e) a bar graph shows the mean percentage of L1CAM-gated events out of total BSE+ events in replicates ($n = 4$) from four different subjects (subtracted by the background signal from the isotype control antibody). In (f), (i) and (l), dot plots overlay the vSSC versus APC signal of BSE-gated events in crude plasma EVs labelled either with BSE alone (light green events) or BSE plus PE-tagged anti-L1CAM antibody (representative vSSC vs. PE fluorescence shown in Figure 4c) and APC-tagged anti-CD9/CD63/CD81 (f), -VAMP2 (i) or -β-III-tubulin (l) antibodies (black events). Colour coded dashed lines designated based on the background signal of negative controls (unlabelled EVs, EVs labelled with an APC-tagged isotype control antibody, and APC-tagged antibodies without EVs) gates events positive for pan-tetraspanins, VAMP2 or β-III-tubulin (events laying on the right of the dashed lines). In (g), (j) and (m), histograms show the number of APC-gated events in f (purple), i (pink) and l (orange), respectively, overlayed with results of EVs labelled with BSE plus APC-tagged isotype control antibody (yellow line). In (h), (k) and (n), dot plots identify the APC signal of L1CAM-gated events (turquoise). In (o), a bar graph shows the mean percentage with standard error of L1CAM-gated events positive for pan-tetraspanins (purple), VAMP2 (pink) and β-III-tubulin (orange) out of total L1CAM-gated events in individual samples from four different subjects. Similar results were obtained in crude plasma EVs isolated by SEC (data not shown).

$2.17 \pm 0.06 \times 10^3$ events per millilitre of crude EVs in Figure 5; $9.57 \pm 3.22 \times 10^4$ events per millilitre of L1CAM IP eluate in Figure 5.

The detection of L1CAM+ EVs in the L1CAM IP eluate was possible using both the 5G3 (Figure 5d, f, g; Figure S12a) and EPR18750 (Figure S12b,c) antibodies, thus validating the presence of the L1CAM ectodomain on EVs in blood. Multiple negative controls validated the ability of FCA to quantify fluorescently labelled detergent-sensitive membranous nanoparticles over soluble L1CAM, labelling agents alone and unstained EVs (Figure 5e). The enrichment of NDEVs from plasma via L1CAM IP was further confirmed using a previously validated Luminex® intact EV assay (Volpert et al., 2022) showing that tetraspanin+ EVs isolated via L1CAM IP carry the neuron-specific marker growth-associated protein 43 (GAP43) (Figure 5l, m) (https://www.proteinatlas.org/ENSG00000172020-GAP43/tissue).

4 | DISCUSSION

The main objective of this study was to address potential limitations of targeting extracellular epitopes of L1CAM via immunoaffinity capture for the enrichment of circulating NDEVs, a research strategy that has been widely adopted to provide non-invasive blood biomarkers for brain disorders. This approach has been criticised based on evidence of L1CAM expression by multiple cell types in the periphery, and L1CAM secretion via proteolytic membrane shedding. These alternative mechanisms of L1CAM release could supply the blood with non-neuronal L1CAM+ EVs and free L1CAM peptides, respectively, interfering with the recovery of NDEVs via L1CAM immunocapture and limiting the potential of this methodology to provide biomarkers specifically reflecting neuronal states. To address these criticisms, we assessed the physical association of L1CAM with the external surface of NDEVs and the level of enrichment achieved by L1CAM immunocapture using FCA and additional techniques at the single-EV level.

First, we validated the sorting of L1CAM extraluminal epitopes to EVs secreted by murine neurons and human iNeurons. Immunoblots targeting L1CAM extracellular epitopes FNIII repeats 1 and 2 (Figure S2a) showed that the predominant species conserved in rat and human neurons are the full-length protein (labelled with an asterisk in Figure 1c) and a variant migrating between 160 and 125 kDa (labelled with an arrowhead in Figure 1c) matching a previously reported 140 kDa product of proteolytic cleavage by the proprotease convertase PC5A that is retained intracellularly in complex with uncleaved, membrane-bound, L1CAM (Kalus et al., 2003). Among these two species, full-length L1CAM was enriched in iNDEV lysates, suggesting that the intact protein is predominantly sorted to NDEVs over intracellular proteolytic products that might escape EV biogenesis pathways in neurons. Additional results obtained by fluorescent confocal microscopy and FCA confirmed the sorting of L1CAM extraluminal epitopes to bona fide single NDEVs carrying the canonical EV markers Alix and tetraspanins CD9, CD63 and CD81 (Figure 1d–o). Particularly, FCA results showed that a vast majority of L1CAM+ EVs from iNeurons co-express the synaptic protein VAMP2 (Figure 1o), previously reported to be enriched in EVs secreted by mice, rat and human neurons (Vilcaes et al., 2021; You et al., 2022), and differentiating them from glia-derived EVs (You et al., 2022; Zhang et al., 2023). Our findings at the single EV level validate previous studies detecting L1CAM in EVs from neuronal culture media via immunoblotting, L1CAM Simoa® of SEC EV fractions and mass spectrometry (Faure et al., 2006; Lachenal et al., 2011; Norman et al., 2021; Vilcaes et al., 2021). In contrast, in a recent proteomics study, L1CAM was not detected in iNeuron-derived EVs (iNDEVs) (You et al., 2022). The discrepancy could be due to the differential centrifugation used for EV isolation in that study, which resulted in discarding large iNDEVs sedimented at 10K (You et al., 2022); our FCA indicates that such an approach could effectively deplete samples of a vast sub-population of larger L1CAM+ EVs (Figure S5). Notably, the same study reported the presence of L1CAM in EVs

20013078, 2024, 6, Downloaded from https://isevjournals.onlinelibrary.wiley.com/doi/10.1002/jev2.12459 by National Health And Medical Research Council, Wiley Online Library on [05/06/2025]. See the Terms and Conditions (https://onlinelibrary.wiley.com/terms-and-conditions) on Wiley Online Library for rules of use; OA articles are governed by the applicable Creative Commons License

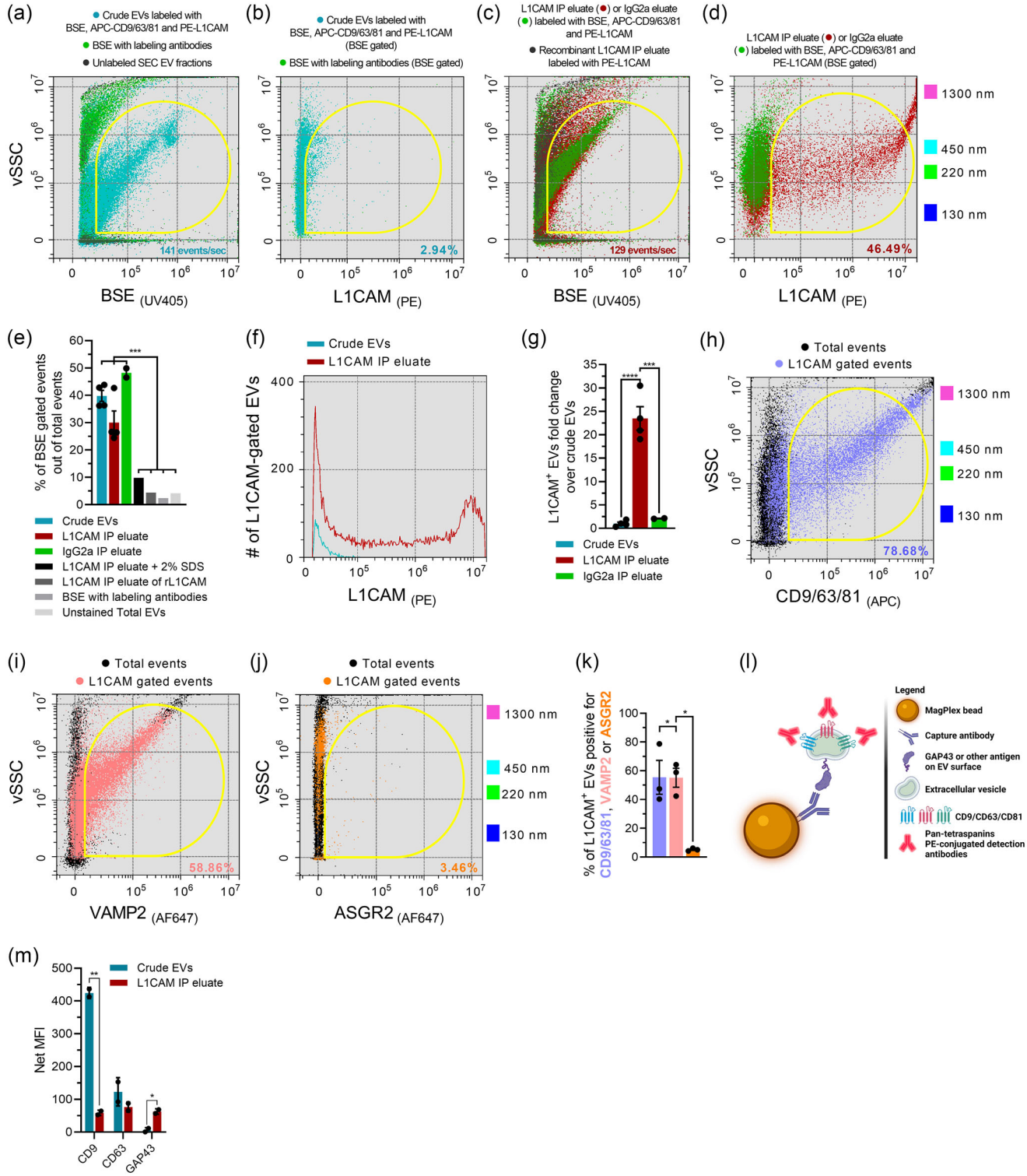

FIGURE 5 L1CAM-IP of human plasma results in the enrichment of L1CAM+ NDEVs. (a–d) Dot plots show the vSSC in function of the fluorescent signal of samples consisting of crude EVs from pooled SEC fractions 1–5 (a and b, turquoise events) or the L1 IP eluate of crude EVs (c and d, dark red events) triple-labelled with the fluorescent EV marker BSE (shown in a and c), and fluorescent antibodies against L1CAM (shown in b and d) and either a mix of antibodies against CD9, CD63, CD81 (pan-tetraspanins), VAMP2 or ASGR2 (shown in h–j, respectively). Yellow gates enclosing events positive for a given marker were designated based on the background signal of negative controls (green and black events). The frequency of events (events/s) in analysed samples, presented in graphs (a) and (c), did not result in coinciding events as confirmed by swarming experiments (Figure S4c,d). Dot plots (b) and (d) include the percentage of BSE-gated events double-positive for L1CAM. (e) Bar graph showing the average percentage of BSE-gated events out of total events in the indicated samples from multiple subjects. (f) A histogram shows the abundance of L1CAM-gated events in (b) and (d). (g) The average number of

(Continues)

20013078, 2024, 6, Downloaded from https://isevjournals.onlinelibrary.wiley.com/doi/10.1002/jev2.12459 by National Health And Medical Research Council, Wiley Online Library on [05/06/2025]. See the Terms and Conditions (https://onlinelibrary.wiley.com/terms-and-conditions) on Wiley Online Library for rules of use; OA articles are governed by the applicable Creative Commons License

FIGURE 5 (Continued)

L1CAM-gated events in the L1CAM IP eluate from multiple subjects is represented as fold-change over crude EVs ($n = 4$ consisting of samples in (b) and (d), from the pooled plasma of two subjects, and samples from the plasma of three subjects assessed individually and shown in Figure S11a), using the eluate of an IP carried with an isotype control for the L1CAM IP antibody as a negative control. (h–j) Dot plots of events identified in the L1CAM IP eluate illustrate the percentage of L1CAM-gated events, shown in colours, double-positive for the indicated EV markers (enclosed by yellow gates). (k) Bar graph showing the average of (h)–(j) from multiple subjects. A colour-coded size range based on the vSSC of FITC-tagged beads (Figure S3a) is included on the right of (d), (h) and (j) for the size comparison of events. Data in (e), (g) and (k) represents the average of separate and pooled samples from multiple subjects ($N = 3$) processed and analysed in three individual experiments. Statistical analyses: one-way ANOVA; $^{*}p < 0.05$, $^{***}p < 0.001$, $^{****}p < 0.0001$; for **e**, the average of negative controls in grey was compared with the other experimental groups (l), A diagram illustrates a Luminex® assay for the detection of EVs positive for GAP43, CD9 or CD63 in crude EVs isolated via SEC before and after L1CAM IP (created with BioRender; agreement number: ZJ23W0UUXG). Recorded mean fluorescence intensity (MFI) signals are graphed in (m) (statistical analysis: unpaired *t*-test; $^{*}p < 0.05$, $^{**}p < 0.005$; average sample replicates from two different subjects with similar results obtained in a separate experiment using samples from additional donors).

isolated from human brain tissue using the same differential ultracentrifugation protocol, suggesting that brain neurons sort L1CAM to smaller EVs at a higher rate than iNeurons. Our findings showing a comparable but higher proportion of L1CAM-positive NDEVs among smaller than among larger blood-borne EVs (Figure S8) are consistent with findings of You et al. (You et al., 2022) for brain-derived EVs, but not for iNDEVs. It seems that iNeurons do not fully replicate the biology of brain neurons, potentially due to differences in the tridimensional structure, at least in terms of NDEV biogenesis, and hence, results based on iNDEVs should be interpreted with caution and validated *ex vivo* and if possible, in vivo.

Previous studies evaluating the sorting of L1CAM to brain-derived NDEVs *ex vivo* include efforts by Norman et al. (2021) describing a Simoa® immunoassay for the quantitation of free and EV-associated L1CAM in SEC-fractionated cerebrospinal fluid (CSF). The results shared in the main manuscript show the predominant co-elution of L1CAM with soluble proteins in late SEC fractions, interpreted by the authors to mean that L1CAM is not associated with brain-derived NDEVs eluting in early SEC fractions (Norman et al., 2021). However, results shared as supplementary material show extrapolated concentrations in all SEC fractions collected, and signals above the lowest quantifiable calibrator in 11 out of the 12 SEC fractions collected, including early fractions containing purified EVs, in agreement with observations reported by another research team (Dutta et al., 2023). These observations can only mean that CSF (which contains EVs more reflective of choroid plexus secretion (Balusu et al., 2016) than of brain interstitial fluid composition) contains higher levels of free than EV-associated L1CAM, although clearly both exist. Moreover, the overrepresentation of soluble L1CAM in CSF might be attributed to contamination with blood, known to carry high levels of free L1CAM as shown by previous results (Norman et al., 2021; Zander et al., 2011) confirmed here (Figure 3a), and expected to occur frequently during standard lumbar punctures (Petzold et al., 2006). Although further studies may be required to elucidate the differential contribution of multiple neuronal secretory pathways to the extracellular L1CAM pool, results provided by Normal et al. suggest its association with EVs, which is confirmed by the assessment of three independent proteomic studies detecting extracellular L1CAM epitopes in brain- and blood-derived EVs (Table 1).

Whilst multiple lines of evidence from human iNeurons, CSF and brain tissue indicate the sorting of L1CAM to brain-derived NDEVs, previous efforts to confirm the physical association of L1CAM with circulating NDEVs are scarce and absent at the single-EV level. We began addressing this knowledge gap by reproducing the Simoa® immunoassay described by Norman et al. (2021) for the unbiased detection of free and EV-associated L1CAM in SEC-fractionated plasma (named here L1CAM/L1CAM Simoa®). We reproduced their results showing the predominant co-elution of L1CAM with soluble proteins in late SEC fractions, with a quantifiable concentration associated with EV markers in early SEC fractions (Figure 2d,e). Immunoblots of human plasma confirmed that a vast majority of free L1CAM circulates as fragments of lower molecular weight (Figure 3a) potentially shed from the membrane of L1CAM-expressing cells. Results indicate that L1CAM circulates in the human blood mainly as extracellular proteolytic fragments at a concentration of 3,634 ± 943 picograms per millilitre of plasma (pg/mL) (based on the L1CAM/L1CAM Simoa® results in SEC fractions 5–13; Figure 2e), with a small fraction carried by EVs at a concentration of 3.2 ± 0.7 pg/mL (based on results in SEC fractions 1–4). Two observations rule out that the detection of L1CAM in early SEC EV fractions is a result of contaminating free L1CAM fragments co-fractionated with EV-associated proteins, instead of true EV cargo. First, the most abundant soluble contaminants were undetected in these early SEC fractions (Figure 2a), including albumin which is ~600-fold more abundant than L1CAM in blood (40 g/L compared to 67 μg/L; https://www.proteinatlas.org). Second, our novel L1CAM/pan-tetraspanins Simoa®, the signal of which is dependent on immunocapturing the L1CAM ectodomain on intact EVs and using antibodies against the three canonical EV tetraspanins for detection (Figure 2d), provided positive results in early SEC EV fractions (Figure 2f). The specificity of our L1CAM/pan-tetraspanins Simoa® towards EV-associated L1CAM over free L1CAM was confirmed by: 1) the much higher signal in crude plasma EVs compared to EV-depleted plasma (Figure 2h); 2) the much lower signal upon treatment of crude plasma EVs with RIPA detergent lysing EVs (Figure 2h); and 3) the signal decrease observed with the addition of recombinant L1CAM competing with L1CAM+ EVs for immunocapture (Figure S7d). The physical association of the L1CAM ectodomain with blood-borne EVs was confirmed by three different techniques at the single EV level, including TEM (Figure 2g), fluorescent confocal microscopy (Figure 2i) and FCA, the latter determining that 3.7 ± 0.9% of total EVs in circulation carry L1CAM (average of results in Figure 4e). *A posteriori* analyses of multiple proteomic studies confirmed that the L1CAM ectodomain is an active cargo of EVs isolated from human brains and plasma (Table 1).

20013078, 2024, 6, Downloaded from https://isevjournals.onlinelibrary.wiley.com/doi/10.1002/jev2.12459 by National Health And Medical Research Council, Wiley Online Library on [05/06/2025]. See the Terms and Conditions (https://onlinelibrary.wiley.com/terms-and-conditions) on Wiley Online Library for rules of use; OA articles are governed by the applicable Creative Commons License

The sub-EV localization of L1CAM is fundamental to its utility as a target for the immunoaffinity isolation of NDEVs from blood, which in turn is subject to its sorting to the extraluminal surface of EVs. Hence, one of the main objectives of our study was to assess the extraluminal localization of L1CAM in EVs from cultured neurons and plasma-derived EVs using multiple techniques and approaches. The reported detection of L1CAM via immunoblotting (Figures 1c and S2b,c), fluorescent confocal microscopy (Figures 1d,e and 2i), FCA (Figures 1f–o, 4, 5a–k, S2d, S5g–l, S8d and S12) and TEM (Figure 2g) was based on the use of antibodies targeting different regions of the L1CAM ectodomain (Figure S2a) whose orientation to the extracellular space of neurons (Jacob et al., 2002; Kenwrick et al., 2000; Maten et al., 2019) is predicted to be preserved in NDEVs. However, these observations do not elucidate the sub-EV localization of L1CAM as immunoblotting results originated from EV protein extracts after membrane lysis, whereas microscopy and FCA observations were made under conditions of partial membrane permeabilization that could allow detection antibodies to bind the L1CAM ectodomain in the EV lumen.

Experiments designed with the purpose of elucidating the sub-EV localization of the L1CAM ectodomain should consider the following plausible scenarios that could limit the utility of L1CAM as a target for the immunoaffinity isolation of NDEVs. First, it has been shown that the topology of some integral membrane proteins could be prone to inversion during sorting to EVs (Cvjetkovic et al., 2016), a scenario that will cause the L1CAM ectodomain to be concealed in the EV lumen. Any experiments seeking to separate the lumen from the membrane of EVs to demonstrate the sub-EV localization of L1CAM would not address the possibility of inversed epitopes, thus offering limited value to the main objective of this study. Also, the cytoplasmic expression of an L1CAM isoform lacking the transmembrane domain (Angiolini et al., 2019) could result in the intravesicular sorting of the L1CAM ectodomain.

Multiple experiments in the present study address these possibilities, as the outcomes are dependent on the exposure of the L1CAM ectodomain on the surface of intact EVs derived from human induced pluripotent stem cell-derived neurons (iNDEVs) and blood. For example, the newly-developed L1CAM/pan-tetraspanin Simoa® assay produces signal from the capture of intact EVs by antibodies targeting the L1CAM ectodomain (Figure 2d), and showed high values when loaded with intact iNDEVs (Figures 2f and S5m) and plasma-derived intact EVs isolated by ExoQuick® sedimentation (Figure 2h), SEC (Figure 2f) and UC (Figure S8c). The significant signal increase observed on the L1CAM/pan-tetraspanin Simoa® (Figure 2h) and FCA (Figure 5g) after subjecting intact plasma EVs to L1CAM IP further confirmed the extraluminal sorting of L1CAM.

To our knowledge, our FCA strategy provides the first clues regarding the sub-cellular and cellular origins of single L1CAM+ EVs in blood. Results summarised in Figure 4o revealed that the majority of peripheral L1CAM+ EVs, specifically 67.4 ± 5.6%, co-carry at least one of the main tetraspanins characterising EVs, CD9, CD63 and CD81. These tetraspanins are mainly involved in the biogenesis of intracellular endosome-derived multivesicular bodies, from where small EVs, termed exosomes, are secreted upon fusion with the plasma membrane (Dixson et al., 2023). However, proteomic findings showing that tetraspanin+ EV sub-populations are enriched in proteins with plasma membrane functions strongly suggest that they are also carried by EVs of larger average size budding from the plasma membrane known as ectosomes (Kowal et al., 2016). These observations support the mixed exosomal and ectosomal identity of L1CAM+ EVs in blood, in line with additional FCA results showing the detection of L1CAM in both small and large plasma-derived EVs (Figure S8d). Interestingly, a third of the peripheral EV pool carrying L1CAM cannot be shown to express CD9, CD63 and CD81. Recently, it was shown that tetraspanins are not expressed on all EV types and have diverse expression between cell types (Kugeratski et al., 2021). Hence, L1CAM+/tetraspanin- events potentially constitute non-classical exosomes carrying other EV markers, the sub-cellular origins of which remain to be elucidated (Jeppesen et al., 2019; Kowal et al., 2016).

Regarding the cellular origin of L1CAM+ EVs in blood, it can be inferred from our results that a high percentage of these originate from neurons based on the co-detection of L1CAM with the neuronal markers β-III-tubulin, VAMP2 and GAP43. These targets were carefully selected based on their enriched neuronal expression compared to peripheral cells (https://www.proteinatlas.org), and previous evidence validating their sorting to EVs from human iNeurons and brains (Vilcaes et al., 2021; You et al., 2022). Our FCA results provide the first quantitative proof of total L1CAM+ EVs in human blood, as well as sub-populations carrying neuronally-enriched markers. The FCA data collected indicated that L1CAM+ EVs constitute 3.75% ± 0.86% of total blood-derived BSE+ EVs, whereas L1CAM+ EVs co-carrying VAMP2 and β-III-tubulin make up 1.26 ± 0.29% and 2.06 ± 0.63%, respectively (mean ± standard deviation) (Figure 4). The detection of β-III-tubulin was performed under conditions of partial membrane permeabilization using a concentration of Tween-20 detergent previously shown to not affect EV morphology (Osteikoetxea et al., 2015) and confirmed here to significantly increase the detection of the intraluminal EV marker Syntenin-1 whilst maintaining the signal of membrane pan-tetraspanins unchanged (Figure S10). These results support the use of non-ionic detergents for the detection of intravesicular markers via FCA and lay the foundation for future studies aimed at developing EV fixation and permeabilization methods granting intraluminal access to other EV markers and compatible with downstream analyses. The specificity of L1CAM as an NDEV marker is further supported by results showing that the percentage of L1CAM- EVs carrying VAMP2 and β-III-tubulin is below 4% (Figure S11). FCA of plasma EVs fractionated by differential UC suggests that L1CAM+ NDEVs are predominantly smaller in size (hence, more likely of endosomal origin), as in the 120K pellet approximately two thirds of EVs carrying L1CAM were double-positive for β-III-tubulin compared to one third in the 10K pellet (Figure S8d). However, a different distribution may be found in EVs with sizes below the current FCA limit resolution of 100 nm based on size calibration using fluorescent nanobeads (Figure S3a).

20013078, 2024, 6, Downloaded from https://isevjournals.onlinelibrary.wiley.com/doi/10.1002/jev2.12459 by National Health And Medical Research Council, Wiley Online Library on [05/06/2025]. See the Terms and Conditions (https://onlinelibrary.wiley.com/terms-and-conditions) on Wiley Online Library for rules of use; OA articles are governed by the applicable Creative Commons License

The partial (about 3.5%) but substantial degree of circulating L1CAM+ EVs is in agreement with previous reports (Kumar et al., 2022; You et al., 2023), and reinforces the rationale for L1CAM immunocapture to derive blood-based biomarkers for neurological and psychiatric disorders. FCA of plasma EVs recovered via L1CAM immunocapture showed a multifold enrichment of L1CAM+ nanoparticles (Figure 5a–g) co-expressing EV and neuronal markers based on the co-detection of major tetraspanins and VAMP2 (Figure 5h, i and k), respectively. The isolation of L1CAM+ EVs via L1CAM immunocapture was confirmed by our L1CAM/pan-tetraspanins Simoa® showing that the abundance of particles co-carrying L1CAM and tetraspanins CD9, CD63 and/or CD81 in the L1CAM IP eluate is many-fold increased compared to crude plasma EVs (Figure 2h). Additional results using a previously validated Luminex® intact EV assay (Volpert et al., 2022) (Figure 5m) support the neuronal nature of L1CAM+ EVs in blood by showing that L1CAM immunocapture targets EVs carrying GAP43, a membrane encored protein highly enriched in brain neurons both at the mRNA and protein levels (https://www.proteinatlas.org/ENSG00000172020-GAP43/tissue) that has been previously shown to be sorted to EVs from human cultured neurons (Anastasi et al., 2021). The co-detection of L1CAM and GAP43 in circulating NDEVs is consistent with previous observations showing that GAP43 immunocapture of plasma-derived EVs results in the enrichment of L1CAM and additional neuronal markers, including PSD95, neurofilament light, synaptophysin and enolase 2, among others (Erez et al., 2023).

The main L1CAM antibody studied here was clone 5G3, as it is commonly used for the immunocapture of NDEVs due to its high reactivity towards the extracellular domain hypothesised to be exposed at the EV surface. The specificity of the 5G3 antibody towards extraluminal L1CAM was confirmed by FCA of intact EVs derived from WT and L1CAM KO HeLa cells, showing reactivity only towards WT EVs (Figure S2c,d). 5G3 is highly reactive towards an L1CAM epitope spanning the extracellular Ig-like domains (Ig) 1 and 2 in a folded conformation dependent on the phosphorylation of amino acid T1172 located at the intracellular cytoplasmic domain (Chen et al., 2010). Dephosphorylation of T1172 results in the unfolding of the extracellular domain and exposure of Ig 1–2 for multimerization upon binding with Ig 3–4, significantly reducing the reactivity of the 5G3 L1CAM antibody. The conformation-dependent binding of 5G3 is supported by FCA (Figure 1i,m), Simoa® (Figure 2e,f), confocal microscopy (Figure 1e) and immunoblotting (Figure S2b) results showing increased reactivity towards neuronal L1CAM under native and non-reducing conditions, in line with previous observations (Rathjen & Schachner, 1984). These observations suggest that most neuronal L1CAM is in the phosphorylated folded conformation accessible for binding by 5G3. On the other hand, L1CAM expressed by CD4+ T-lymphocytes is only detected by the L1CAM antibody clone UJ127 (Ebeling et al., 1996; Pancook et al., 1997) with high affinity towards the extracellular fibronectin-type III repeat 4 that, contrary to the 5G3 ligand spanning the Ig 1–2 domains, is concealed in the phosphorylated folded conformation, exposed upon T1172 dephosphorylation, and remains accessible after multimerization (Chen et al., 2010). Interestingly, the UJ127 ligand spans the binding site of the protease ADAM10 regulating the membrane proximal cleavage of L1CAM (Linneberg et al., 2019). These observations suggest that the conformational equilibrium of L1CAM from some peripheral sources might be shifted towards dephosphorylated unfolded configurations prone to proteolytic cleavage by membrane proteases, thus conveying specificity to the 5G3 antibody towards neuronal L1CAM.

Another molecular event that should increase the specificity of the 5G3 antibody towards NDEVs immunocapture is the alternative splicing of the L1CAM mRNA. Whilst neurons predominantly express the full-length variant of L1CAM, non-neuronal cells, such as Schwann cells, kidney cells and blood lymphocytes, express a short isoform of L1CAM lacking exons 2 and 27 mediating neural growth and L1CAM internalization, respectively (Schafer & Altevogt, 2010). Of note, exon 27, excluded from the non-neural transcript, encodes the YRSL sequence mediating receptor endocytosis via clathrin-coated pits upon binding to the clathrin adaptor AP-2 (Kamiguchi et al., 1998). Given that clathrin-mediated endocytosis is known to be a key pathway of EV biogenesis regulating the sorting of membrane receptors to early endosomes (Gurung et al., 2021), it is plausible that non-neural L1CAM lacking exon 27 is not sorted to endosome-derived exosomes. Additionally, it was recently reported that endothelial cells express an L1CAM isoform lacking the transmembrane domain (L1CAM-ΔTM) encoded in exon 25 (Angiolini et al., 2019). Due to the absence of the transmembrane sequence, L1CAM-ΔTM cannot be sorted to the plasma membrane and is secreted to the extracellular milieu in its free form regulating angiogenic functions (Angiolini et al., 2019).

The cell-specific structural configuration, membrane shedding and alternative splicing of L1CAM suggests that in EVs from peripheral sources, the L1CAM extraluminal epitope targeted by the 5G3 antibody is either concealed or absent. Hence, L1CAM+ EVs from non-neuronal cells might not represent an overwhelming confounding factor in the affinity isolation of NDEVs from blood. Multiple additional lines of evidence concur, including the proteomics profiling of plasma EVs isolated via L1CAM IP detecting the ectodomain of L1CAM in association with multiple brain-enriched and neuronal proteins (Table 1), and our FCA showing that more than 50% of peripheral L1CAM+ EVs detected by the 5G3 antibody carry the canonical neuronal marker β-III-tubulin (Figures 4l–o and S8d). Additional FCA results for plasma EVs recovered via L1CAM immunocapture concur with this theory, showing that whilst the percentage of L1CAM+ EVs co-carrying pan-tetraspanins was similar before (67.4 ± 5.6%; Figure 4o) and after (55.4 ± 20.4%; Figure 5k) L1CAM immunocapture, L1CAM+ EVs double-positive for VAMP2 of potential neuronal origin increased from 33.6 ± 3.6% to 55.13 ± 11.39%. Based on these results, about one third of EVs recovered via L1CAM immunocapture may be secreted by non-neuronal cells. This dual origin limits to a degree but does not negate the potential of L1CAM immunocapture to provide blood-based biomarkers for neurological and psychiatric disorders. Another potential confounding factor limiting the utility of this methodology to provide biomarkers specific for brain disorders is the recovery of EVs

20013078, 2024, 6, Downloaded from https://isevjournals.onlinelibrary.wiley.com/doi/10.1002/jev2.12459 by National Health And Medical Research Council, Wiley Online Library on [05/06/2025]. See the Terms and Conditions (https://onlinelibrary.wiley.com/terms-and-conditions) on Wiley Online Library for rules of use; OA articles are governed by the applicable Creative Commons License

from peripheral neurons expressing L1CAM. We previously demonstrated that EVs recovered through 5G3 L1CAM immunocapture contain only full length L1CAM, similar to brain lysate; in contrast, total EVs in circulation contain additional lower molecular weight fragments (see Figure S1c in Vreones, M. et al. (2023)). Moreover, the correlation of EV cargo in L1CAM IP eluates with brain pathology in mice (Delgado-Peraza et al., 2021) suggests that the potential interference of contaminating EV subpopulations is not imposing. Nevertheless, alternative immunocapture or sorting strategies to either reduce the load of non-neuronal EVs (negative selection) or increase that of neuronal EVs (positive selection) might improve the accuracy, sensitivity, and specificity of this diagnostic approach. Recent efforts from our group and others aim to accomplish this objective by evaluating additional targets for the immunoaffinity isolation of blood-borne NDEVs, such as ATPase Na+/K+ transporting subunit alpha 3 (ATP1A3), GAP43, and neuroligin 3 (NLGN3) (Erez et al., 2023; You et al., 2023).

Another concern that has been raised against the use of L1CAM as a target for the immunoaffinity isolation of blood-borne NDEVs is the presence of high concentrations of free L1CAM in the circulation. Free forms of full-length L1CAM and extracellular proteolytic peptides are readily detected in plasma and serum as shown by previous results (Norman et al., 2021; Zander et al., 2011) confirmed here (Figure 3a). Such high concentrations of soluble L1CAM in plasma could interfere with the immunoaffinity capture of NDEVs by competing with L1CAM+ EVs for binding to L1CAM capture antibodies. Our results showing the 25-fold enrichment of L1CAM+ EVs from plasma via L1CAM IP suggest that this is mitigated by clearing soluble L1CAM from crude plasma EVs by ExoQuick® sedimentation (Figure 2h) or SEC (Figure 5) prior to immunoaffinity capture. Free forms of L1CAM in plasma could also mediate the recovery of non-specific EVs upon binding to the protein corona of redundant EVs. We directly addressed this possibility by showing that full-length L1CAM and its ectodomain-containing products present in EV-depleted plasma were not adsorbed by the protein corona of HEK-derived EVs, in contrast to the circulating lipoprotein ApoA1 (Figure 3). These findings agree with the predominant hypothesis that the adsorption of soluble components by the protein corona of plasma EVs is regulated by specific receptor-ligand interactions rather than resulting from non-specific binding, and that some proteins viewed as contaminants in EV preparations from blood, like for example ApoA1, might be inherent components of peripheral EVs (Toth et al., 2021).

In conclusion, our study provides evidence from multiple single-vesicle analyses validating the existence of an L1CAM+ EV sub-population in human blood co-carrying multiple neuronally-enriched (albeit, not entirely neuron-specific) markers, including GAP43, β-III-tubulin and VAMP2, that became enriched via L1CAM IP. The results presented identify neurons as a main source of L1CAM+ EVs in blood amidst other potential cellular sources and support the utility of L1CAM as a target for the isolation of NDEVs from blood.

To further assess the CNS origin of L1CAM+ EVs in blood, future studies may explore if these carry additional markers showing high levels of expression in neurons and low levels of expression in peripheral cells based on data from omics repositories. However, this approach has its own limitations. For example, the proteomic profiling of EVs from human neurons and brain tissue show that not every neuronal marker showing brain specificity is sorted to NDEVs (You et al., 2022). On the other hand, our FCA findings open the window for an alternative approach to characterise the cellular origins of peripheral EV sub-populations carrying potential NDEV markers based on their sorting at the single-EV level to provide samples with the purity and yield required for cross-referencing omics data for brain and peripheral tissues from publicly available repositories. Of note, irrespectively of the degree of brain specificity of L1CAM or any other NDEV target, its utility as a source of biomarkers is ultimately dependent on clinical evidence demonstrating the diagnostic potential of derived biomarkers for brain disorders, as done extensively over the years for L1CAM+ EVs.

To reach these conclusions we followed experimental practices (detailed at the end of the methods section) that comply with established guidelines to improve the reliability and reproducibility of EV studies (Théry et al., 2018; Welsh et al., 2020), confirming that our observations arise from EVs rather than confounding elements. Although our FCA results suggest that after L1CAM IP we derive an enriched population of NDEVs, a degree of contamination with non-neuronal L1CAM+ EVs represents a limitation; thus, ongoing methods development should aim to provide even purer NDEVs and validate achieved progress with methods as rigorous as here against the L1CAM benchmark. Future research on EV biomarkers should employ single-vesicle analyses to corroborate the cellular source of EVs carrying biomarkers of interest. Despite limitations, our results reinforce the rationale for using L1CAM IP to derive NDEVs from blood, an approach with documented success in biomarker discovery for multiple brain diseases.

AUTHOR CONTRIBUTIONS

Carlos J Nogueras-Ortiz: Conceptualization; data curation; formal analysis; investigation; methodology; validation; visualization; writing—original draft; writing—review & editing. **Erden Eren**: Data curation; investigation; methodology. **Pamela Yao**: Investigation; methodology. **Elizabeth Calzada**: Data curation; formal analysis; investigation; methodology. **Christopher Dunn**: Methodology. **Olga Volpert**: Investigation; methodology. **Francheska Delgado-Peraza**: Investigation; methodology; writing—review and editing. **Maja Mustapic**: Investigation; methodology; writing—review and editing. **Alexey Lyashkov**: Investigation; methodology. **F Javier Rubio**: Methodology; writing—review and editing. **Michael Vreones**: Investigation. **Lesley Cheng**: Investigation; writing—review and editing. **Yang You**: Investigation. **Andrew F Hill**: Investigation; resources. **Tsuneya Ikezu**: Investigation; resources; writing—review and editing. **Erez Eitan**: Investigation; methodology; resources;

20013078, 2024, 6, Downloaded from https://isevjournals.onlinelibrary.wiley.com/doi/10.1002/jev2.12459 by National Health And Medical Research Council, Wiley Online Library on [05/06/2025]. See the Terms and Conditions (https://onlinelibrary.wiley.com/terms-and-conditions) on Wiley Online Library for rules of use; OA articles are governed by the applicable Creative Commons License

supervision; writing—review and editing. **Edward J Goetzl**: Methodology; supervision; writing—review and editing. **Dimitrios Kapogiannis**: Conceptualization; funding acquisition; investigation; methodology; project administration; resources; supervision; visualization; writing—review and editing.

ACKNOWLEDGEMENTS

We would like to extend our gratitude to the following individuals for providing advice and materials: Dr. Christopher Ramsden from NIA/NIH for providing iNeurons; Dr. Charysse Vandendriessche from VIB-UGent Centre for Inflammation Research for assisting in the characterization of EVs using ExoView™ and Dr. Anto Praveen Rajkumar Rajamani from the University of Nottingham and the Nanoscale and Microscale Research Centre of the University of Nottingham for acquiring the Cryo-TEM images. This work was supported by the Intramural Research Program of the National Institute on Aging (NIA), National Institutes of Health (NIH).

CONFLICT OF INTEREST STATEMENT

Carlos J. Nogueras-Ortiz, Erden Eren, Pamela Yao, Elizabeth Calzada, Christopher Dunn, Francheska Delgado-Peraza, Maja Mustapic, Alexey Lyashkov, F. Javier Rubio, Michael Vreones, Lesley Cheng, Yang You, Andrew F Hill, Tsuneya Ikezu and Dimitrios Kapogiannis declare no conflict of interest. Edward J. Goetzl has filed an application with the U.S. Patent Office for the isolation methodology of neuron and astrocyte derived extracellular vesicles. Erez Eitan is a shareholder and employee of NeuroDex, Inc. Olga Volpert is an employee of NeuroDex, Inc.

ORCID

Carlos J Nogueras-Ortiz https://orcid.org/0000-0003-2503-965X
Erden Eren https://orcid.org/0000-0002-5190-9500
Olga Volpert https://orcid.org/0000-0003-1381-5543
Michael Vreones https://orcid.org/0009-0003-1719-8156
Andrew F Hill https://orcid.org/0000-0001-5581-2354
Tsuneya Ikezu https://orcid.org/0000-0002-3979-8596

REFERENCES

Alvarez-Erviti, L., Seow, Y., Yin, H., Betts, C., Lakhal, S., & Wood, M. J. (2011). Delivery of siRNA to the mouse brain by systemic injection of targeted exosomes. *Nature Biotechnology*, *29*(4), 341–345.

Anastasi, F., Masciandaro, S. M., Carratore, R. D., Dell'Anno, M. T., Signore, G., Falleni, A., McDonnell, L. A., & Bongioanni, P. (2021). Proteomics profiling of neuron-derived small extracellular vesicles from human plasma: enabling single-subject analysis. *International Journal of Molecular Sciences*, *22*(6), 2951.

Angiolini, F., Belloni, E., Giordano, M., Campioni, M., Forneris, F., Paronetto, M. P., Lupia, M., Brandas, C., Pradella, D., Di Matteo, A., Giampietro, C., Jodice, G., Luise, C., Bertalot, G., Freddi, S., Malinverno, M., Irimia, M., Moulton, J. D., Summerton, J., … Ghigna, C. (2019). A novel L1CAM isoform with angiogenic activity generated by NOVA2-mediated alternative splicing. *Elife*, *8*, e44305.

Balusu, S., Van Wonterghem, E., De Rycke, R., Raemdonck, K., Stremersch, S., Gevaert, K., Brkic, M., Demeestere, D., Vanhooren, V., Hendrix, A., Libert, C., & Vandenbroucke, R. E. (2016). Identification of a novel mechanism of blood-brain communication during peripheral inflammation via choroid plexus-derived extracellular vesicles. *EMBO Molecular Medicine*, *8*(10), 1162–1183.

Bhargava, P., Nogueras-Ortiz, C., Kim, S., Delgado-Peraza, F., Calabresi, P. A., & Kapogiannis, D. (2021). Synaptic and complement markers in extracellular vesicles in multiple sclerosis. *Multiple Sclerosis*, *27*(4), 509–518.

Blommer, J., Pitcher, T., Mustapic, M., Eren, E., Yao, P. J., Vreones, M. P., Pucha, K. A., Dalrymple-Alford, J., Shoorangiz, R., Meissner, W. G., Anderson, T., & Kapogiannis, D. (2023). Extracellular vesicle biomarkers for cognitive impairment in Parkinson's disease. *Brain*, *146*(1), 195–208.

Chen, M. M., Lee, C. Y., Leland, H. A., Lin, G. Y., Montgomery, A. M., & Silletti, S. (2010). Inside-out regulation of L1 conformation, integrin binding, proteolysis, and concomitant cell migration. *Molecular Biology of the Cell*, *21*(10), 1671–1685.

Cvjetkovic, A., Jang, S. C., Konecna, B., Hoog, J. L., Sihlbom, C., Lasser, C., & Lotvall, J. (2016). Detailed analysis of protein topology of extracellular vesicles-evidence of unconventional membrane protein orientation. *Scientific Reports*, *6*, 36338.

Delgado-Peraza, F., Nogueras-Ortiz, C., Simonsen, A. H., Knight, D. D., Yao, P. J., Goetzl, E. J., Jensen, C. S., Hogh, P., Gottrup, H., Vestergaard, K., Hasselbalch, S. G., & Kapogiannis, D. (2023). Neuron-derived extracellular vesicles in blood reveal effects of exercise in Alzheimer's disease. *Alzheimer's Research & Therapy*, *15*(1), 156.

Delgado-Peraza, F., Nogueras-Ortiz, C. J., Volpert, O., Liu, D., Goetzl, E. J., Mattson, M. P., Greig, N. H., Eitan, E., & Kapogiannis, D. (2021). Neuronal and astrocytic extracellular vesicle biomarkers in blood reflect brain pathology in mouse models of Alzheimer's disease. *Cells*, *10*(5), 993.

Dickens, A. M., Tovar, Y. R. L. B., Yoo, S. W., Trout, A. L., Bae, M., Kanmogne, M., Megra, B., Williams, D. W., Witwer, K. W., Gacias, M., Tabatadze, N., Cole, R. N., Casaccia, P., Berman, J. W., Anthony, D. C., & Haughey, N. J. (2017). Astrocyte-shed extracellular vesicles regulate the peripheral leukocyte response to inflammatory brain lesions. *Science Signaling*, *10*(473), eaai7696.

Dixson, A. C., Dawson, T. R., Di Vizio, D., & Weaver, A. M. (2023). Context-specific regulation of extracellular vesicle biogenesis and cargo selection. *Nature Reviews Molecular Cell Biology*, *24*(7), 454–476.

Dutta, S., Hornung, S., Taha, H. B., & Bitan, G. (2023). Biomarkers for parkinsonian disorders in CNS-originating EVs: Promise and challenges. *Acta Neuropathologica*, *145*(5), 515–540.

Ebeling, O., Duczmal, A., Aigner, S., Geiger, C., Schollhammer, S., Kemshead, J. T., Moller, P., Schwartz-Albiez, R., & Altevogt, P. (1996). L1 adhesion molecule on human lymphocytes and monocytes: Expression and involvement in binding to alpha v beta 3 integrin. *European Journal of Immunology*, *26*(10), 2508–2516.

20013078, 2024, 6, Downloaded from https://isevjournals.onlinelibrary.wiley.com/doi/10.1002/jev2.12459 by National Health And Medical Research Council, Wiley Online Library on [05/06/2025]. See the Terms and Conditions (https://onlinelibrary.wiley.com/terms-and-conditions) on Wiley Online Library for rules of use; OA articles are governed by the applicable Creative Commons License

Erez, E., Tricia, T.-W., Katya, E., Eren, E., Eve, G., Amir, L., Olga, V., Mitra, A., Daniel, G. S., & Dimitrios, K. (2023). Synaptic proteins in neuron-derived extracellular vesicles as biomarkers for Alzheimer's disease: Novel methodology and clinical proof of concept. *Extracellular Vesicles and Circulating Nucleic Acids*, *4*(1), 133–150.

Faure, J., Lachenal, G., Court, M., Hirrlinger, J., Chatellard-Causse, C., Blot, B., Grange, J., Schoehn, G., Goldberg, Y., Boyer, V., Kirchhoff, F., Raposo, G., Garin, J., & Sadoul, R. (2006). Exosomes are released by cultured cortical neurones. *Molecular and Cellular Neuroscience*, *31*(4), 642–648.

Fiandaca, M. S., Kapogiannis, D., Mapstone, M., Boxer, A., Eitan, E., Schwartz, J. B., Abner, E. L., Petersen, R. C., Federoff, H. J., Miller, B. L., & Goetzl, E. J. (2015). Identification of preclinical Alzheimer's disease by a profile of pathogenic proteins in neurally derived blood exosomes: A case-control study. *Alzheimers & Dementia*, *11*(6), 600–607e1.

Fowler, C. D. (2019). NeuroEVs: Characterizing extracellular vesicles generated in the neural domain. *Journal of Neuroscience*, *39*(47), 9262–9268.

Fu, Y., Jiang, C., Tofaris, G. K., & Davis, J. J. (2020). Facile impedimetric analysis of neuronal exosome markers in Parkinson's Disease dagnostics. *Analytical Chemistry*, *92*(20), 13647–13651.

Ghosh, S., Bhowmik, S., Majumdar, S., Goswami, A., Chakraborty, J., Gupta, S., Aggarwal, S., Ray, S., Chatterjee, R., Bhattacharyya, S., Dutta, M., Datta, S., Chowdhury, A., Dhali, G. K., & Banerjee, S. (2020). The exosome encapsulated microRNAs as circulating diagnostic marker for hepatocellular carcinoma with low alpha-fetoprotein. *International Journal of Cancer*, *147*(10), 2934–2947.

Goetzl, E. J., Srihari, V. H., Mustapic, M., Kapogiannis, D., & Heninger, G. R. (2022). Abnormal levels of mitochondrial Ca(2+) channel proteins in plasma neuron-derived extracellular vesicles of early schizophrenia. *Faseb Journal*, *36*(8), e22466.

Gomes, D. E., & Witwer, K. W. (2022). L1CAM-associated extracellular vesicles: A systematic review of nomenclature, sources, separation, and characterization. *Journal of Extracellular Biology*, *1*(3), e35.

Gomes, P. A., Bodo, C., Nogueras-Ortiz, C., Samiotaki, M., Chen, M., Soares-Cunha, C., Silva, J. M., Coimbra, B., Stamatakis, G., Santos, L., Panayotou, G., Tzouanou, F., Waites, C. L., Gatsogiannis, C., Sousa, N., Kapogiannis, D., Costa-Silva, B., & Sotiropoulos, I. (2023). A novel isolation method for spontaneously released extracellular vesicles from brain tissue and its implications for stress-driven brain pathology. *Cell Communication and Signaling*, *21*(1), 35.

Gurung, S., Perocheau, D., Touramanidou, L., & Baruteau, J. (2021). The exosome journey: From biogenesis to uptake and intracellular signalling. *Cell Communication and Signaling*, *19*(1), 47.

Hill, A. F. (2019). Extracellular Vesicles and Neurodegenerative Diseases. *Journal of Neuroscience*, *39*(47), 9269–9273.

Jacob, J., Haspel, J., Kane-Goldsmith, N., & Grumet, M. (2002). L1 mediated homophilic binding and neurite outgrowth are modulated by alternative splicing of exon 2. *Journal of Neurobiology*, *51*(3), 177–189.

Jeppesen, D. K., Fenix, A. M., Franklin, J. L., Higginbotham, J. N., Zhang, Q., Zimmerman, L. J., Liebler, D. C., Ping, J., Liu, Q., Evans, R., Fissell, W. H., Patton, J. G., Rome, L. H., Burnette, D. T., & Coffey, R. J. (2019). Reassessment of Exosome Composition. *Cell*, *177*(2), 428–445. e18.

Jiang, C., Hopfner, F., Katsikoudi, A., Hein, R., Catli, C., Evetts, S., Huang, Y., Wang, H., Ryder, J. W., Kuhlenbaeumer, G., Deuschl, G., Padovani, A., Berg, D., Borroni, B., Hu, M. T., Davis, J. J., & Tofaris, G. K. (2020). Serum neuronal exosomes predict and differentiate Parkinson's disease from atypical parkinsonism. *Journal of Neurology, Neurosurgery, and Psychiatry*, *91*(7), 720–729.

Kalus, I., Schnegelsberg, B., Seidah, N. G., Kleene, R., & Schachner, M. (2003). The proprotein convertase PC5A and a metalloprotease are involved in the proteolytic processing of the neural adhesion molecule L1. *Journal of Biological Chemistry*, *278*(12), 10381–10388.

Kamiguchi, H., Long, K. E., Pendergast, M., Schaefer, A. W., Rapoport, I., Kirchhausen, T., & Lemmon, V. (1998). The neural cell adhesion molecule L1 interacts with the AP-2 adaptor and is endocytosed via the clathrin-mediated pathway. *Journal of Neuroscience*, *18*(14), 5311–5321.

Kapogiannis, D., Dobrowolny, H., Tran, J., Mustapic, M., Frodl, T., Meyer-Lotz, G., Schiltz, K., Schanze, D., Rietschel, M., Bernstein, H. G., & Steiner, J. (2019). Insulin-signaling abnormalities in drug-naive first-episode schizophrenia: Transduction protein analyses in extracellular vesicles of putative neuronal origin. *European Psychiatry*, *62*, 124–129.

Kapogiannis, D., Mustapic, M., Shardell, M. D., Berkowitz, S. T., Diehl, T. C., Spangler, R. D., Tran, J., Lazaropoulos, M. P., Chawla, S., Gulyani, S., Eitan, E., An, Y., Huang, C. W., Oh, E. S., Lyketsos, C. G., Resnick, S. M., Goetzl, E. J., & Ferrucci, L. (2019). Association of extracellular vesicle biomarkers with Alzheimer disease in the Baltimore longitudinal study of aging. *JAMA neurology*, *76*(11), 1340–1351.

Kenwrick, S., Watkins, A., & De Angelis, E. (2000). Neural cell recognition molecule L1: Relating biological complexity to human disease mutations. *Human Molecular Genetics*, *9*(6), 879–886.

Kowal, J., Arras, G., Colombo, M., Jouve, M., Morath, J. P., Primdal-Bengtson, B., Dingli, F., Loew, D., Tkach, M., & Thery, C. (2016). Proteomic comparison defines novel markers to characterize heterogeneous populations of extracellular vesicle subtypes. *PNAS*, *113*(8), E968–E977.

Kugeratski, F. G., Hodge, K., Lilla, S., McAndrews, K. M., Zhou, X., Hwang, R. F., Zanivan, S., & Kalluri, R. (2021). Quantitative proteomics identifies the core proteome of exosomes with syntenin-1 as the highest abundant protein and a putative universal biomarker. *Nature Cell Biology*, *23*(6), 631–641.

Kumar, A., Sharma, M., Su, Y., Singh, S., Hsu, F. C., Neth, B. J., Register, T. C., Blennow, K., Zetterberg, H., Craft, S., & Deep, G. (2022). Small extracellular vesicles in plasma reveal molecular effects of modified Mediterranean-ketogenic diet in participants with mild cognitive impairment. *Brain Communications*, *4*(6), fcac262.

Lachenal, G., Pernet-Gallay, K., Chivet, M., Hemming, F. J., Belly, A., Bodon, G., Blot, B., Haase, G., Goldberg, Y., & Sadoul, R. (2011). Release of exosomes from differentiated neurons and its regulation by synaptic glutamatergic activity. *Molecular and Cellular Neuroscience*, *46*(2), 409–418.

Lewczuk, P., Riederer, P., O'Bryant, S. E., Verbeek, M. M., Dubois, B., Visser, P. J., Jellinger, K. A., Engelborghs, S., Ramirez, A., Parnetti, L., Jack, C. R., Jr, Teunissen, C. E., Hampel, H., Lleó, A., Jessen, F., Glodzik, L., de Leon, M. J., Fagan, A. M., Molinuevo, J. L., … Kornhuber, J., Members of the WFSBP Task Force Working on this Topic: Peter Riederer, Carla Gallo, Dimitrios Kapogiannis, Andrea Lopez Mato, Florence Thibaut. (2018). Cerebrospinal fluid and blood biomarkers for neurodegenerative dementias: An update of the consensus of the task force on biological markers in psychiatry of the World Federation of Societies of Biological Psychiatry. *The World Journal of Biological Psychiatry: The Official Journal of the World Federation of Societies of Biological Psychiatry*, *19*(4), 244–328.

Libregts, S., Arkesteijn, G. J. A., Nemeth, A., Nolte-'t Hoen, E. N. M., & Wauben, M. H. M. (2018). Flow cytometric analysis of extracellular vesicle subsets in plasma: Impact of swarm by particles of non-interest. *Journal of Thrombosis and Haemostasis*, *16*(7), 1423–1436.

Linneberg, C., Toft, C. L. F., Kjaer-Sorensen, K., & Laursen, L. S. (2019). L1cam-mediated developmental processes of the nervous system are differentially regulated by proteolytic processing. *Scientific Reports*, *9*(1), 3716.

Lutz, D., Wolters-Eisfeld, G., Joshi, G., Djogo, N., Jakovcevski, I., Schachner, M., & Kleene, R. (2012). Generation and nuclear translocation of sumoylated transmembrane fragment of cell adhesion molecule L1. *Journal of Biological Chemistry*, *287*(21), 17161–17175.

Maten, M. V., Reijnen, C., Pijnenborg, J. M. A., & Zegers, M. M. (2019). L1 cell adhesion molecule in cancer, a systematic review on domain-specific functions. *International Journal of Molecular Sciences*, *20*(17), 4180.

Mechtersheimer, S., Gutwein, P., Agmon-Levin, N., Stoeck, A., Oleszewski, M., Riedle, S., Postina, R., Fahrenholz, F., Fogel, M., Lemmon, V., & Altevogt, P. (2001). Ectodomain shedding of L1 adhesion molecule promotes cell migration by autocrine binding to integrins. *Journal of Cell Biology*, *155*(4), 661–673.

20013078, 2024, 6, Downloaded from https://isevjournals.onlinelibrary.wiley.com/doi/10.1002/jev2.12459 by National Health And Medical Research Council, Wiley Online Library on [05/06/2025]. See the Terms and Conditions (https://onlinelibrary.wiley.com/terms-and-conditions) on Wiley Online Library for rules of use; OA articles are governed by the applicable Creative Commons License

Mitsuhashi, M., Taub, D. D., Kapogiannis, D., Eitan, E., Zukley, L., Mattson, M. P., Ferrucci, L., Schwartz, J. B., & Goetzl, E. J. (2013). Aging enhances release of exosomal cytokine mRNAs by Abeta1-42-stimulated macrophages. *Faseb Journal*, *27*(12), 5141–5150.

Morales-Kastresana, A., Telford, B., Musich, T. A., McKinnon, K., Clayborne, C., Braig, Z., Rosner, A., Demberg, T., Watson, D. C., Karpova, T. S., Freeman, G. J., DeKruyff, R. H., Pavlakis, G. N., Terabe, M., Robert-Guroff, M., Berzofsky, J. A., & Jones, J. C. (2017). Labeling extracellular vesicles for nanoscale flow cytometry. *Scientific Reports*, *7*(1), 1878.

Mullins, R. J., Mustapic, M., Goetzl, E. J., & Kapogiannis, D. (2017). Exosomal biomarkers of brain insulin resistance associated with regional atrophy in Alzheimer's disease. *Human Brain Mapping*, *38*(4), 1933–1940.

Mustapic, M., Eitan, E., Werner, J. K., Jr., Berkowitz, S. T., Lazaropoulos, M. P., Tran, J., Goetzl, E. J., & Kapogiannis, D. (2017). Plasma extracellular vesicles enriched for neuronal origin: A potential window into brain pathologic processes. *Frontiers in neuroscience*, *11*, 278.

Nasca, C., Dobbin, J., Bigio, B., Watson, K., de Angelis, P., Kautz, M., Cochran, A., Mathe, A. A., Kocsis, J. H., Lee, F. S., Murrough, J. W., McEwen, B. S., & Rasgon, N. (2021). Insulin receptor substrate in brain-enriched exosomes in subjects with major depression: On the path of creation of biosignatures of central insulin resistance. *Molecular Psychiatry*, *26*(9), 5140–5149.

Niu, M., Li, Y., Li, G., Zhou, L., Luo, N., Yao, M., Kang, W., & Liu, J. (2020). A longitudinal study on alpha-synuclein in plasma neuronal exosomes as a biomarker for Parkinson's disease development and progression. *European Journal of Neurology*, *27*(6), 967–974.

Nogueras-Ortiz, C. J., Mahairaki, V., Delgado-Peraza, F., Das, D., Avgerinos, K., Eren, E., Hentschel, M., Goetzl, E. J., Mattson, M. P., & Kapogiannis, D. (2020). Astrocyte- and neuron-derived extracellular vesicles from Alzheimer's disease patients effect complement-mediated neurotoxicity. *Cells*, *9*(7), 1618.

Norman, M., Ter-Ovanesyan, D., Trieu, W., Lazarovits, R., Kowal, E. J. K., Lee, J. H., Chen-Plotkin, A. S., Regev, A., Church, G. M., & Walt, D. R. (2021). L1CAM is not associated with extracellular vesicles in human cerebrospinal fluid or plasma. *Nature Methods*, *18*(6), 631–634.

Osteikoetxea, X., Sodar, B., Nemeth, A., Szabo-Taylor, K., Paloczi, K., Vukman, K. V., Tamasi, V., Balogh, A., Kittel, A., Pallinger, E., & Buzas, E. I. (2015). Differential detergent sensitivity of extracellular vesicle subpopulations. *Organic & Biomolecular Chemistry*, *13*(38), 9775–9782.

Pancook, J. D., Reisfeld, R. A., Varki, N., Vitiello, A., Fox, R. I., & Montgomery, A. M. (1997). Expression and regulation of the neural cell adhesion molecule L1 on human cells of myelomonocytic and lymphoid origin. *Journal of Immunology*, *158*(9), 4413–4421.

Peltz, C. B., Kenney, K., Gill, J., Diaz-Arrastia, R., Gardner, R. C., & Yaffe, K. (2020). Blood biomarkers of traumatic brain injury and cognitive impairment in older veterans. *Neurology*, *95*(9), e1126–e1133.

Petzold, A., Sharpe, L. T., & Keir, G. (2006). Spectrophotometry for cerebrospinal fluid pigment analysis. *Neurocritical Care*, *4*(2), 153–162.

Pulliam, L., Liston, M., Sun, B., & Narvid, J. (2020). Using neuronal extracellular vesicles and machine learning to predict cognitive deficits in HIV. *Journal of Neurovirology*, *26*(6), 880–887.

Pulliam, L., Sun, B., Mustapic, M., Chawla, S., & Kapogiannis, D. (2019). Plasma neuronal exosomes serve as biomarkers of cognitive impairment in HIV infection and Alzheimer's disease. *Journal of Neurovirology*, *25*(5), 702–709.

Rathjen, F. G., & Schachner, M. (1984). Immunocytological and biochemical characterization of a new neuronal cell surface component (L1 antigen) which is involved in cell adhesion. *Embo Journal*, *3*(1), 1–10.

Rufino-Ramos, D., Lule, S., Mahjoum, S., Ughetto, S., Cristopher Bragg, D., Pereira de Almeida, L., Breakefield, X. O., & Breyne, K. (2022). Using genetically modified extracellular vesicles as a non-invasive strategy to evaluate brain-specific cargo. *Biomaterials*, *281*, 121366.

Schafer, M. K., & Altevogt, P. (2010). L1CAM malfunction in the nervous system and human carcinomas. *Cellular and Molecular Life Sciences*, *67*(14), 2425–2437.

Shi, M., Liu, C., Cook, T. J., Bullock, K. M., Zhao, Y., Ginghina, C., Li, Y., Aro, P., Dator, R., He, C., Hipp, M. J., Zabetian, C. P., Peskind, E. R., Hu, S. C., Quinn, J. F., Galasko, D. R., Banks, W. A., & Zhang, J. (2014). Plasma exosomal alpha-synuclein is likely CNS-derived and increased in Parkinson's disease. *Acta Neuropathologica*, *128*(5), 639–650.

Skog, J., Wurdinger, T., van Rijn, S., Meijer, D. H., Gainche, L., Sena-Esteves, M., Curry, W. T., Jr., Carter, B. S., Krichevsky, A. M., & Breakefield, X. O. (2008). Glioblastoma microvesicles transport RNA and proteins that promote tumour growth and provide diagnostic biomarkers. *Nature Cell Biology*, *10*(12), 1470–1476.

Sun, B., Dalvi, P., Abadjian, L., Tang, N., & Pulliam, L. (2017). Blood neuron-derived exosomes as biomarkers of cognitive impairment in HIV. *Aids*, *31*(14), F9–F17.

Tauro, B. J., Greening, D. W., Mathias, R. A., Ji, H., Mathivanan, S., Scott, A. M., & Simpson, R. J. (2012). Comparison of ultracentrifugation, density gradient separation, and immunoaffinity capture methods for isolating human colon cancer cell line LIM1863-derived exosomes. *Methods (San Diego, Calif.)*, *56*(2), 293–304.

Théry, C., Witwer, K. W., Aikawa, E., Alcaraz, M. J., Anderson, J. D., Andriantsitohaina, R., Antoniou, A., Arab, T., Archer, F., Atkin-Smith, G. K., Ayre, D. C., Bach, J. M., Bachurski, D., Baharvand, H., Balaj, L., Baldacchino, S., Bauer, N. N., Baxter, A. A., Bebawy, M., … Zuba-Surma, E. K. (2018). Minimal information for studies of extracellular vesicles 2018 (MISEV2018): A position statement of the International Society for Extracellular Vesicles and update of the MISEV2014 guidelines. *Journal of Extracellular Vesicles*, *7*(1), 1535750.

Toth, E. A., Turiak, L., Visnovitz, T., Cserep, C., Mazlo, A., Sodar, B. W., Forsonits, A. I., Petovari, G., Sebestyen, A., Komlosi, Z., Drahos, L., Kittel, A., Nagy, G., Bacsi, A., Denes, A., Gho, Y. S., Szabo-Taylor, K. E., & Buzas, E. I. (2021). Formation of a protein corona on the surface of extracellular vesicles in blood plasma. *Journal of Extracellular Vesicles*, *10*(11), e12140.

Vandendriessche, C., Kapogiannis, D., & Vandenbroucke, R. E. (2022). Biomarker and therapeutic potential of peripheral extracellular vesicles in Alzheimer's disease. *Advanced Drug Delivery Reviews*, *190*, 114486.

Vassileff, N., Vella, L. J., Rajapaksha, H., Shambrook, M., Kenari, A. N., McLean, C., Hill, A. F., & Cheng, L. (2020). Revealing the proteome of motor cortex derived extracellular vesicles isolated from amyotrophic lateral sclerosis human postmortem tissues. *Cells*, *9*(7), 1709.

Vella, L. J., Scicluna, B. J., Cheng, L., Bawden, E. G., Masters, C. L., Ang, C. S., Willamson, N., McLean, C., Barnham, K. J., & Hill, A. F. (2017). A rigorous method to enrich for exosomes from brain tissue. *Journal of Extracellular Vesicles*, *6*(1), 1348885.

Vilcaes, A. A., Chanaday, N. L., & Kavalali, E. T. (2021). Interneuronal exchange and functional integration of synaptobrevin via extracellular vesicles. *Neuron*, *109*(6), 971–983 e5.

Volpert, O. V., Gershun, E., Elgart, K., Kalia, V., Wu, H., Baccarelli, A. A., Eren, E., Kapogiannis, D., Verma, A., Levin, A., & Eitan, E. (2022). Novel modification of Luminex assay for characterization of extracellular vesicle populations in biofluids. *BioRxiv*. https://doi.org/10.1101/2022.01.12.475897

Vreones, M., Mustapic, M., Moaddel, R., Pucha, K. A., Lovett, J., Seals, D. R., Kapogiannis, D., & Martens, C. R. (2023). Oral nicotinamide riboside raises NAD+ and lowers biomarkers of neurodegenerative pathology in plasma extracellular vesicles enriched for neuronal origin. *Aging Cell*, *22*(1), e13754.

Walker, K. A., Chawla, S., Nogueras-Ortiz, C., Coresh, J., Sharrett, A. R., Wong, D. F., Jack, C. R., Jr., Spychalla, A. J., Gottesman, R. F., & Kapogiannis, D. (2021). Neuronal insulin signaling and brain structure in nondemented older adults: The Atherosclerosis Risk in Communities Study. *Neurobiology of Aging*, *97*, 65–72.

20013078, 2024, 6, Downloaded from https://isevjournals.onlinelibrary.wiley.com/doi/10.1002/jev2.12459 by National Health And Medical Research Council, Wiley Online Library on [05/06/2025]. See the Terms and Conditions (https://onlinelibrary.wiley.com/terms-and-conditions) on Wiley Online Library for rules of use; OA articles are governed by the applicable Creative Commons License

Welsh, J. A., Van Der Pol, E., Arkesteijn, G. J. A., Bremer, M., Brisson, A., Coumans, F., Dignat-George, F., Duggan, E., Ghiran, I., Giebel, B., Görgens, A., Hendrix, A., Lacroix, R., Lannigan, J., Libregts, S. F. W. M., Lozano-Andrés, E., Morales-Kastresana, A., Robert, S., De Rond, L., … Jones, J. C. (2020). MIFlowCyt-EV: A framework for standardized reporting of extracellular vesicle flow cytometry experiments. *Journal of Extracellular Vesicles*, *9*(1), 1713526.

You, Y., Muraoka, S., Jedrychowski, M. P., Hu, J., McQuade, A. K., Young-Pearse, T., Aslebagh, R., Shaffer, S. A., Gygi, S. P., Blurton-Jones, M., Poon, W. W., & Ikezu, T. (2022). Human neural cell type-specific extracellular vesicle proteome defines disease-related molecules associated with activated astrocytes in Alzheimer's disease brain. *Journal of Extracellular Vesicles*, *11*(1), e12183.

You, Y., Zhang, Z., Sultana, N., Ericsson, M., Martens, Y. A., Sun, M., Kanekiyo, T., Ikezu, S., Shaffer, S. A., & Ikezu, T. (2023). ATP1A3 as a target for isolating neuron-specific extracellular vesicles from human brain and biofluids. *Science Advances*, *9*(37), eadi3647.

Zander, H., Rawnaq, T., von Wedemeyer, M., Tachezy, M., Kunkel, M., Wolters, G., Bockhorn, M., Schachner, M., Izbicki, J. R., & Kaifi, J. (2011). Circulating levels of cell adhesion molecule L1 as a prognostic marker in gastrointestinal stromal tumor patients. *BMC Cancer*, *11*(189), 1–7.

Zhang, Z., Yu, K., You, Y., Jiang, P., Wu, Z., DeTure, M. A., Dickson, D. W., Ikezu, S., Peng, J., & Ikezu, T. (2023). Comprehensive characterization of human brain-derived extracellular vesicles using multiple isolation methods: Implications for diagnostic and therapeutic applications. *Journal of Extracellular Vesicles*, *12*(8), e12358.

SUPPORTING INFORMATION

Additional supporting information can be found online in the Supporting Information section at the end of this article.

How to cite this article: Nogueras-Ortiz, C. J., Eren, E., Yao, P., Calzada, E., Dunn, C., Volpert, O., Delgado-Peraza, F., Mustapic, M., Lyashkov, A., Rubio, F. J., Vreones, M., Cheng, L., You, Y., Hill, A. F., Ikezu, T., Eitan, E., Goetzl, E. J., & Kapogiannis, D. (2024). Single-extracellular vesicle (EV) analyses validate the use of L1 Cell Adhesion Molecule (L1CAM) as a reliable biomarker of neuron-derived EVs. *Journal of Extracellular Vesicles*, *13*, e12459. https://doi.org/10.1002/jev2.12459

20013078, 2024, 6, Downloaded from https://isevjournals.onlinelibrary.wiley.com/doi/10.1002/jev2.12459 by National Health And Medical Research Council, Wiley Online Library on [05/06/2025]. See the Terms and Conditions (https://onlinelibrary.wiley.com/terms-and-conditions) on Wiley Online Library for rules of use; OA articles are governed by the applicable Creative Commons License